AN ELECTRON-ELECTRON COINCIDENCE SPECTROMETER AND THE DECAY OF Os^{193}.

AN ELECTRON-ELECTRON COINCIDENCE SPECTROMETER AND THE DECAY OF Os^{193}

by

EDWIN E. HABIB, B.Sc.

A Thesis

Submitted to the Faculty of Graduate Studies
in Partial Fulfilment of the Requirements
for the degree
Doctor of Philosophy

McMaster University

May 1961

DOCTOR OF PHILOSOPHY (1961) McMASTER UNIVERSITY
(Physics) Hamilton, Ontario.

TITLE: An Electron-Electron Coincidence Spectrometer and the Decay of Os^{193}

AUTHOR: Edwin E. Habib, B. Sc. (University of Birmingham)

SUPERVISOR: Professor M. W. Johns

NUMBER OF PAGES: x, 72

SCOPE AND CONTENTS: The design and construction of a coincidence spectrometer and its application to the study of the decay of Os^{193} are presented.

ACKNOWLEDGEMENTS

I would like to express my appreciation to Professor Martin W. Johns for his guidance and instruction throughout the duration of this work.

My gratitude is due to the members of my supervisory committee, Dr. A. B. McLay, Dr. R. H. Tomlinson and Dr. M. W. Johns for their interest and advice, and I would like to acknowledge the part played by Dr. M. E. Law in the planning and execution of the experiments. I would like to express my thanks to Mr. Thomas Bryden and Mr. William McMicking of the machine shop for the parts they played in the construction of the instrument.

The assistance of Mr. Robert Price in recording the data and the advice of Miss Agda Artna on the techniques of source preparations are also acknowledged.

I am also grateful to Mrs. Susanna Allon and Mr. W. Grewe for preparing the drawings for the thesis.

I am indebted to the National Research Council and to McMaster University for financial support in the form of scholarships. This project has been steadily supported by research grants from the National Research Council.

TABLE OF CONTENTS

FIGURE INDEX

LIST OF TABLES

PREFACE

The study of beta decay has played an important role in Nuclear Physics from the early years of this century to the present time. The experiments of von Baeyer (1), of Chadwick (2) and of Rutherford (3) over the period extending from 1910 to 1914 had revealed the three main components of the radiation in beta decay. The group of electrons of continuous energy distribution was identified with the disintegration of the nucleus, and the monoenergetic groups of electrons and the gamma rays were thought to be connected with the reorganization of the new nucleus formed (4). This latter view was finally confirmed in 1922. Over the next decade the efforts directed to the study of the disintegration electrons culminated in 1934 in the theory of beta decay proposed by Fermi. Since 1934, the use of artificially produced radio isotopes and improved experimental techniques have provided confirmation of this theory and yielded new information concerning nuclear processes. In the Fermi theory the disintegration energy is shared between an electron and a neutrino. This latter particle, assumed to have zero charge and mass and postulated simply to conserve momentum and energy, interacts so weakly with matter that its direct detection did not occur until 1956. In that year, Reines and Cowan (5) demonstrated the presence of inverse beta decay induced by the large anti-neutrino flux from a nuclear reactor. About the same time the suggestion of Lee and Yang (6) that parity might not be conserved

in beta decay led to a flurry of experiments which determined the coupling constants of beta decay and provided new insight into the spin properties of the neutrino. A study of a specific beta decay process can yield information concerning nuclear matrix elements, and the spins and parities of nuclear levels in both the parent and daughter nuclides. These studies are therefore useful in providing the new material for testing existing nuclear models and suggesting modifications to them.

The work described in this thesis is concerned with the construction of an electron-electron coincidence spectrometer designed for studying the generic relationships between various beta and conversion electron groups in beta decay, determining conversion probabilities and measuring branching ratios. This spectrometer has then been used to study Os^{193} which decays by beta decay to Ir^{193} with a 31-hour half-life. The decay scheme of this nuclide has been extremely difficult to solve because there are many excited states of Ir^{193} in a small energy range and none of these are strongly populated in the beta decay process.

The first chapter gives a brief account of the theoretical concepts necessary for an understanding of the thesis. Subsequent chapters deal in turn with the theory of operation of beta ray spectrometers and coincidence experiments, the details of construction of the electron-electron spectrometer and the results of the experiments on Os^{193}.

CHAPTER I

(i) Introduction

A nuclear level is characterized by its energy, spin and parity. These quantities are not directly observable but are inferred from a study of its transitions to other nuclear levels. In the beta decay process, the transition is from a level in the nucleus (A,Z) to a level in the nucleus (A , Z + 1) with the accompanying emission of a negative electron and an antineutrino and the properties of the initial level must be deduced from the nature of the beta spectrum. If the level of interest is an excited state, it may decay to the ground state of the same nucleus by the emission of electromagnetic radiation or conversion electrons. The properties of the initial level must now be deduced from the energies and intensities of these radiations.

(ii) Beta Decay

The Fermi theory is set up in analogy with the process of photon emission by electric charges. The transition probability is given from perturbation theory as

$$T = \frac{2\pi}{\hbar} \left| H_{int} \right|^2 \frac{dn}{dE} \qquad (1)$$

where $\left| H_{int} \right|$ is the interaction Hamiltonian and $\frac{dn}{dE}$ is the density of final states.

In the case of photon emission, the Hamiltonian density is

$$\rho\phi - \frac{1}{c}\underline{j}\cdot\underline{A}$$

where ρ and $\underline{j}$ are the source charge and current densities and Φ and $\underline{A}$ are the electromagnetic scalar and vector potentials respectively. The quantities $(\underline{j}\ ,\ ic\rho)$ and $(\underline{A}\ ,\ i\Phi)$ are both four vectors. The Hamiltonian is then a scalar product of two vectors and the interaction is called a vector interaction. To form the analagous two four-vectors in beta decay (which is the form Fermi first constructed in his theory) the wave functions of the nucleus and leptons (electron and neutrino) are used. The Hamiltonian is

$$Hv = g\left[(\Psi_f^*\Psi_i)(\psi^*\phi) - (\Psi_f^*\alpha\,\Psi_i)(\psi^*\alpha\,\phi)\right] \qquad (2)$$

It was soon shown that the vector interaction was not the only one possible but that there were four other ways of constructing a relativistically invariant Hamiltonian. Much of the effort of beta ray spectroscopists for the last twenty-five years has gone into attempts to determine which of these five actually occur in nature. The discovery of parity non conservation and the experimental results connected with this discovery have shown that only the vector (v) and axial vector (A) interactions are present in the beta interaction. The Hamiltonian may therefore be written as $H = C_V H_V + C_A H_A$, (3)

where C_A and C_V are coupling constants such that

$$C_A^{\,2} + C_V^{\,2} = 1$$

Since we must sum over all nucleons and integrate over the entire nuclear volume, the final expression for the transition probability becomes

$$T = \frac{2\pi}{\hbar}\left|\sum_k \int H\,\delta(r - r_k)\,d\tau_k\right|^2 \frac{dn}{dE} \qquad (4)$$

The term in the modulus is called a matrix element. The first order term in the expansion of this matrix element, in terms of spherical harmonics gives the transition probability for the so called allowed spectrum. Physically this corresponds to the emission of the leptons with zero orbital angular momentum and therefore no change in parity. For the vector (the so-called Fermi) interaction, the selection rules are

$$\Delta I = 0 \quad , \quad \Delta \pi = 0 .$$

for the axial vector (the so-called Gamow-Teller) interaction, the selection rules are

$$\Delta I = \pm 1 \, , \; (0 \not\to 0) \, , \quad \Delta \pi = 0 .$$

The second term in the expansion is much smaller than the first, and its effects can only be observed if the allowed transition cannot take place. The selection rules in this case (the so-called first forbidden transitions) are

$\Delta I = \pm 1, 0, 0 \not\to 0, \; \Delta \pi = -1$ for the vector interaction

$\Delta I = \pm 2, \pm 1, 0, \quad (0 \not\to 0)$

$\Delta \pi = -1 \quad\quad (0 \not\leftrightarrow 1)$ for the axial vector interaction.

$(1/2 \not\to 1/2)$

The argument can be extended to higher order terms, and leads to second, third, etc, forbidden transitions.

The matrix element for allowed transitions is independent of energy, and we can replace it by a constant. We can get the momentum distribution of the electrons from equation (4) by expressing $\frac{dn}{dE}$ in terms of the momentum and energy of the emitted electron, and including a factor F(E,Z) which corrects for the coulomb effect of the nuclear charge.

We get $P(p) = (g^2/2\pi^3\hbar^7c^3)\,|M_{if}|^2\,F(E,Z)\,p^2(E_{max}-E)^2$

where $|M_{if}|^2$ = matrix element

E_{max} = maximum energy of the emitted electron

g = coupling constant

The shape of the distribution apart from the factor F(E,Z) is determined by $p^2(E_{max} - E)^2$ which is called the statistical factor.

A plot of $\sqrt{\frac{P(p)}{F p^2}}$ versus E is called a Fermi plot and is a straight line with an intercept on the energy axis equal to E_{max}. Spectra which give a linear Fermi plot are said to have the "allowed shape". For forbidden spectra the matrix element is a function of the electron energy and so one would not expect these to have the allowed shape. However, the departures from linearity for most first forbidden spectra are so slight as to be experimentally undetectable. Notable exceptions are the so-called first forbidden unique spectra with $\Delta I = 2$, yes, and Re^{186} with $\Delta I = 1$, yes (7)

The total probability that an electron be emitted is

$\lambda = \int_0^{p_{max}} P(p)\,dp = 0.693/t$ where t is the half-life. The half-life is therefore dependent on the disintegration energy. We can, however, find a quantity called the comparative half-life which is independent of energy, and depends only on the nuclear matrix element. From above, it follows that

$$0.\frac{693}{t} = |M_{if}|^2 \frac{g^2}{2\pi^3\hbar^7c^3} \int_0^{p_{max}} F(Z,E)\,p^2(E_{max}-E)^2\,dp$$

$$= \text{const}\,|M_{if}|^2 f(Z,E)$$

$$\therefore ft = \text{const}\,|M_{if}|^{-2}$$

The range of values of ft, the comparative half-life, is extremely large, so

$\log_{10}$ ft is generally quoted. For allowed transitions $\log_{10}$ ft ranges from 4.0 - 6.0 except for mirror transitions where the value is around 3.5. For first forbidden non unique spectra, $\log_{10}$ ft ranges from 6.5 - 9 while for higher order of forbiddenness, the values are correspondingly higher.

(iii) Electromagnetic Transition

Electromagnetic radiation from nuclei can be classified as dipole, quadrupole, 2^l pole according as to whether one, two or l units of angular momentum are carried away by the photon. For any given multipole order, the radiation may be classified as electric if the parity change is $(-1)^l$ or magnetic if the parity change is $(-1)^{l-1}$. Calculations of transition probabilities can only be carried out in terms of some specific nuclear model. For any model the transition probabilities may be expected to decrease very rapidly with increasing l. This is clearly shown by the formulae for the single particle model (46):

$$T(E) = \frac{4.4(L+1)}{L[(2L+1)!!]^2}\left(\frac{3}{L+3}\right)^2\left(\frac{E_\gamma}{197}\right)^{2L+1} a^{2L} \times 10^{21} \text{ sec}^{-1}$$

$$T(M) = \frac{0.19(L+1)}{L[(2L+1)!!]^2}\left(\frac{3}{L+2}\right)^2\left(\mu_p L - \frac{L}{L+1}\right)^2\left(\frac{E_\gamma}{197}\right)^{2L+1} \times a^{2L-2} \times 10^{21} \text{ sec}^{-1}$$

$a = 1.45 \times 10^{-1/3} A^{1/3}$ in 10^{-13} cm units

$\mu_p = 2.79$, E_γ in Mev.

Consider two levels A and B within the same nucleus. The radiation from A to B will be restricted to those multipoles which satisfy the condition

$$j_A + j_B \geq l \geq j_A - j_B$$

and the parity condition for electric and magnetic radiations. On the basis of the single particle formulae one can arrange the various multipoles in order of decreasing probability according to the following scheme

Type of Radiation	E1	M1	E2	M2	E3	M3	E4	M_4	E_5
Parity change	yes	No		yes		No		yes	

Thus for a transition between two states of specified parity only the lowest allowed multipole order may be expected to contribute appreciably to the intensity of the radiation. This in fact is found to be true except for transitions between states of the same parity and spin difference of $\pm$ 1, or 0 ($0 \not\rightarrow 0$, and $1 \not\leftrightarrow 0$). For these, one would expect pure M1 radiation on the single particle estimate whereas in fact one often finds a mixture of M1 and E2. The enhancement of the E2 intensity is related to the occurence of collective effects in the nucleus.

As an alternative mechanism to photon emission in the de-excitation process the nuclear excitation energy may be transferred directly to an orbital electron which emerges with the transition energy less the orbital binding energy. The absolute probability for this internal conversion process depends on the nuclear model used, but the ratio of the conversion electron to the photon emission probability depends only on the multipole character of the electromagnetic transition. Thus the internal conversion coefficients

$$\alpha_K = \frac{N_{eK}}{N_\gamma}, \quad \alpha_{L_1} = \frac{N_{eL_1}}{N_\gamma}, \text{ etc}$$

and $\frac{K}{L}$, $\frac{L}{M}$, $L_I : L_{II} : L_{III}$ ratios are sensitive functions of the character and energy of the transition. Extensive tables of conversion coefficients are now available (8) and make it possible to use measured conversion coefficients and their ratios to determine the character of the radiations. It is more convenient in the coincidence spectrometer to work directly with conversion probabilities, defined as

$$\mathcal{K}_K = \frac{\alpha_K}{1 + \alpha_K + \alpha_L + \cdots} = \frac{N_{eK}}{N_\gamma + N_{eK} + N_{eL} + \cdots}.$$

(iv) The Nuclear Shell Model

The shell model proposed independently in 1950 by workers in Switzerland (Haxel, Jensen and Suess (9)) and the U.S.A. (Mayer (10)) has had striking success in predicting the properties of the ground states of nuclei. The basis of the model is the assumption that each nucleon moves in the average field due to the rest of the nucleus. The exact nature of the potential is not known but the order of filling the levels is not very sensitive to the choice of potential so long as it is spherically symmetrical (the square well and the harmonic oscillator have been two favourite choices). If one applies the Pauli exclusion principle separately to protons and neutrons, the occupation number for each level is determined and the appearance of closed shells occurs quite naturally. It had long been known that nuclei with 2, 8, 20, 50, 82 and 126 neutrons or protons are particularly stable (Mayer) and these values became known as "magic numbers". Almost any simple potential leads to the closure of shells at 2, 8, and 20 but all of them failed to predict the others. Mayer showed that with the addition of an unexpectedly strong spin-orbit coupling about (fifteen times that expected from the known proton and neutron magnetic moments) the theory could be made to predict closed shells at all of the magic numbers. While this theory has made it possible to predict correctly the ground state spins and parities for elements of mass < 120 (with some exceptions) it is not so successful for the strongly deformed nuclei with partially filled shells. The ground state spins for such nuclei have been much more reliably predicted by Nilsson (41) using an ellipsoidal potential and spin-orbit coupling. In his

treatment, the simple shell model orbits are replaced by orbits characterized by the parity, and the component Ωp of the nucleon angular momentum along the nuclear symmetry axis. Each orbit may be occupied twice, once for $+\Omega p$ and once for $-\Omega p$. The effect of this potential is to mix the simple shell model orbits more and more as the nuclear deformation increases. In this model one might expect to find $_{76}Os_{117}^{193}$ with a ground state of 3/2- and an 11/2+ particle state not too far above it. Similarly $_{77}Ir_{116}^{193}$ should have a 3/2+ ground state spin with low lying particle levels of 1/2+ and 11/2- nearby.

(v) The Unified Model

Even while the successes of the shell model were being exploited its weaknesses became evident. It failed to explain the large quadrupole moments between closed shells and the presence of E2 transitions as much as 100 times faster than the single particle estimates which occurred from low lying nuclear states. The answers to these questions and many others were provided by the unified model of Bohr and Mottelson (11). Large quadrupole moments indicated strongly deformed nuclei and led to a consideration of collective modes of excitation of a spheroidal drop of matter. For a strongly deformed nucleus, the most easily excited mode is that of rotation and its mathematical description is similar to that of the familiar rigid rotator of the molecule. In general one expects a series of energy levels with spins I_o, $I_o + 1$, $I_o + 2$ ..... with energies given by $E_{rot} = \frac{\hbar^2}{2j} I\ (I + 1)$ and all of the same parity. Two special cases occur; if $I_o = 0$, (as is true for all even- even nuclei in the ground state) the spin sequence is 0, 2, 4, 6 ..., while if $I_o = 1/2$ a special correction term of

the form a $(-1)^{I + 1/2}(I + 1/2)$ must be added to E_{rot} to yield the correct energy of the level. It should be noted that the moment of inertia j is not that of a rigid spheroid rotating about its axis, but that of a matter wave moving over a rigid core.

Deformed nuclei may also be made to perform vibrations, i.e. periodic changes in the shape of the surface without a change in volume. These may be classified as β vibrations (those which retain cylindrical symmetry about the axis of symmetry) and γ vibrations (those which are not symmetric about the axis). Nuclei close to the closed shells are very difficult to set in rotation. For these the level structure is more easily described in terms of a three dimensional harmonic oscillator with equally spaced degenerate levels with spins of (0), (2), (0,2,4), (2, 3, 4, 6) etc. In practice, the degeneracy of the pure harmonic oscillator is unlikely to be realized. An interesting extension of the theory of the vibrational levels has been given by Davydov and Philippov (12) who discuss the properties of the levels to be expected for an asymmetric rigid rotator and apply their results to levels in even-even nuclei.

The actual level structure of a heavy nucleus will consist of a combination of particle and vibrational levels, each carrying its own rotational band. Since the levels may be close together, perturbation effects can well wipe out any similarity between the actual levels and those predicted by the model. Only for highly deformed nuclei or those close to the closed shells can the actual structure be easily interpreted.

CHAPTER II

BETA RAY SPECTROMETERS

(i) Introduction

A great deal has been written on the subject of the design, construction and performance of beta ray spectrometers. There are excellent reviews by Kai Siegbahn (13), Persico and Geoffrion (14) and many others. The first published work on the determination of energies in beta radiation was done by O. von Baeyer and O. Hahn in 1910 (15). The deflection of beta particles in a magnetic field was measured by a photographic plate placed at some distance away from a radioactive deposit on a wire. No attempt was made at focussing. Nevertheless, these authors were able to report the presence of definite lines corresponding to monoenergetic groups of electrons in the beta spectrum.

The first semi-circular magnetic spectrometer was built by Danyz (16) in 1912. This instrument consists of a uniform magnetic field in which a source and some detecting device are placed in the same plane perpendicular to the direction of the magnetic field. A narrow beam of electrons, selected by suitable source slits, describes a circular path in this plane and comes to focus after describing a semi-circle. In spite of its inherent low transmission, modern versions of this type of spectrometer are still being used because of their cheapness,

precision and ease of construction. The field can be measured with high accuracy using the proton resonance method and so absolute determinations of energies can be readily made. Photographic registration can be used to compensate for its low transmission, since a large part of the spectrum can be recorded in one exposure. The double focussing spectrometer, first built by Siegbahn and Svartholm (17), is a flat spectrometer like the semi-circular instrument which employs a shaped field to obtain focussing in the z direction (perpendicular to the orbital plane) as well as in the radial direction. Since Div B = 0, and Curl B = 0 for free space, specification of B_z is sufficient to determine B_r and B_o completely.

$$B_z = B_o\left[1 + \frac{\alpha(r-a)}{a} + \beta\left(\frac{r-a}{a}\right)^2 + \gamma\left(\frac{r-a}{a}\right)^3 + \ldots\right].$$

If $\alpha = \beta = \gamma = 0$, we have the situation in the semi-circular spectrometer with no focussing in the z direction. For $\alpha = 1/2$, we have 1st order focussing at $\Theta = \sqrt{2}\,\pi$ for all values of ϕ_r and ϕ_z. This means that the first order terms in ϕ_r and ϕ_z vanish in the equation for the image size. The coefficients β and γ must be adjusted to obtain complete second order focussing. With iron, it is difficult to do this precisely by shaping the pole pieces, and so these instruments fall short of ideal performance. With iron-free instruments it is possible to design the coils to give any desired values of β and γ and eliminate defocussing terms up to the 3rd order. Such an instrument was built by Ewan et al (18) at Chalk River following the design conditions worked out by Lee Whiting (19).

Over the years there has been a corresponding development in spectrometers employing magnetic lenses. In these the magnetic field has axial

symmetry and the elections travel in helical paths. These instruments in general have higher transmission and poorer resolution than the flat instruments and are better suited for coincidence experiments. The first of this type of instrument was made by Tricker (20). Very superior instruments using fields of this general type have been constructed by DuMond (21), Schmidt (22), Siegbahn and Slatis (23), de Waard (24) and Gerholm (25).

The decision to build a Gerholm type instrument at McMaster was dictated by the need to have available an instrument suitable for coincidence work with a resolution sufficient to resolve the complex conversion electron spectra of the heavier nuclei. This instrument is essentially two beta ray spectrometers placed back to back in such a way as to allow them to "look at" a common source. Each half of the instrument has a transmission of about 4% and a resolution of about 1.5% for a source size of 2 mm. Gerholm's paper was not sufficiently detailed to serve as a blue-print and so the construction of the McMaster instrument involved a considerable amount of design. Its principle of operation is discussed in section (vi).

(ii) General Properties of Magnetic Spectrometers

Since the radius of curvature ρ of an electron orbit in a uniform magnetic field B is related to the momentum by the relation $p = B\rho e$, it is customary in experimental work to measure momentum in gauss-cm units. The corresponding electron energies can be calculated directly or obtained more conveniently through the use of tables, (26). Most magnetic spectrometers do not have a constant field over the entire trajectory. Nevertheless, as long as

the source and detector are fixed and suitable baffles are provided to ensure that only electrons in a momentum band Δp about p can pass from the source to the detector, it is still true that the magnetic field at any fixed point in the electron trajectory is proportional to p. Therefore, in any magnetic spectrometer, a measurement of the field at one point can be used as a measure of p. If the instrument is iron-free, a measurement of the magnetizing current is equally as good as a measure of the momentum and much more easily carried out. This feature is one of the great advantages of iron-free instruments over those with iron-shaped fields.

The transmission ω of a spectrometer is defined as the fraction of the electrons of momentum p emitted from the source which arrive at the detector when the instrument is focussed on p. The resolution of a spectrometer is usually determined by observing its response to a source of monoergic electrons. When the counting rate is plotted as a function of the field B, or the momentum p, one obtains response curves of the type shown below.

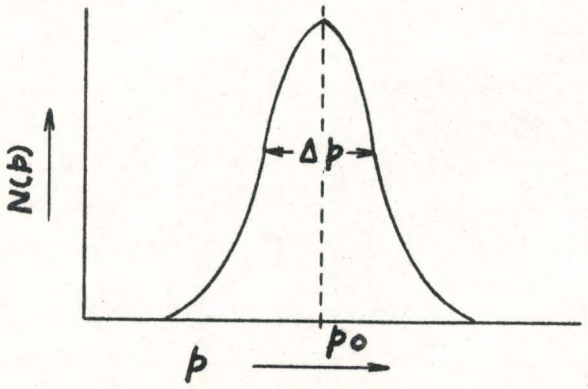

Figure 1

The resolution R is defined as $\frac{\Delta p}{p_0}$ where Δp is the momentum spread at half maximum and p_0 is the momentum at the peak counting rate. R is independent

of ρ_0 . It should be noted that each instrument has its own characteristic line profile determined by its own particular focussing properties, but this definition of R can be used for all of them.

Although both the transmission and the resolution of a spectrometer are independent of p, they both depend strongly on the design of the instrument, the choice of baffles and the source and detector dimensions. In any practical beta ray spectrometer, a compromise must be made between the conflicting requirements of high transmission and low resolution. The ratio R/ω is often called the figure of merit of the instrument. R/ω varies from about 20 for older instruments to 0.1 for many of the best modern instruments (27).

(iii) Ring Focus and Baffles

In a lens spectrometer, the electrons leaving the source at an entrance angle α to the axis eventually return to the axis again to form an image. The spherical aberration of this image is large for many field shapes. A position of minimum spherical aberration generally occurs before the electrons cross the axis at the so-called ring focus. A great improvement in performance is obtained by placing the defining baffles at this focus rather than at the detector (28). Ring focussing is employed in the Gerholm instrument.

In any lens spectrometer, the profile of a mono-energetic line is due to the following three effects acting independently of each other (the broadening due to source thickness ignored),

(1) the finite angle of acceptance of the spectrometer

(2) the finite size of the ring focus gap, which for a fixed angle of emission

accepts a finite momentum interval

(3) the finite size of the source.

Du Mond (29) and Persico (30) have discussed in detail the case of the homogeneous field lens spectrometer and Du Mond has established a criterion for the optimum source size, instrumental resolution and transmission with an arrangement of diaphragms shown in Figure 2 below.

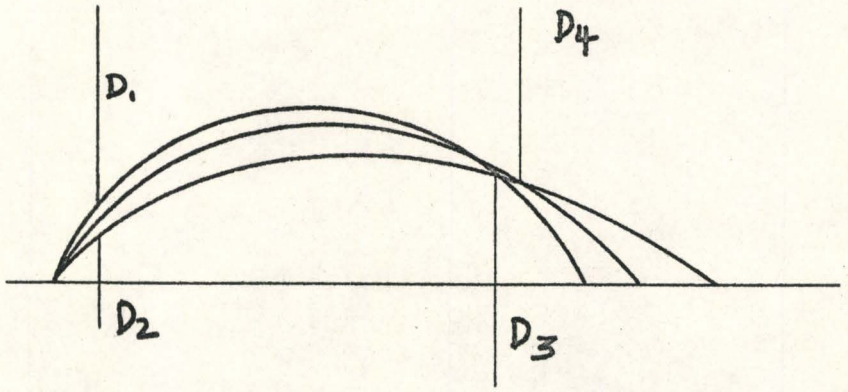

Figure 2

The diaphragms D_1 and D_2 define the solid angle and D_3 and D_4 the momentum band for a fixed angle of emission. Du Mond has suggested that for a given transmission, the width of the ring focus be such that broadening at the base of the resolution curve due to finite transmission, momentum and resolution be approximately equal. The source size should then be chosen to give an equal base broadening. Hubert (31) has shown that the arrangement of diaphragms shown below in Figure 3 leads to an improvement in resolution for the same transmission. The combination of diaphragms D_1, D_2, D_3 define both the solid angle and the momentum band.

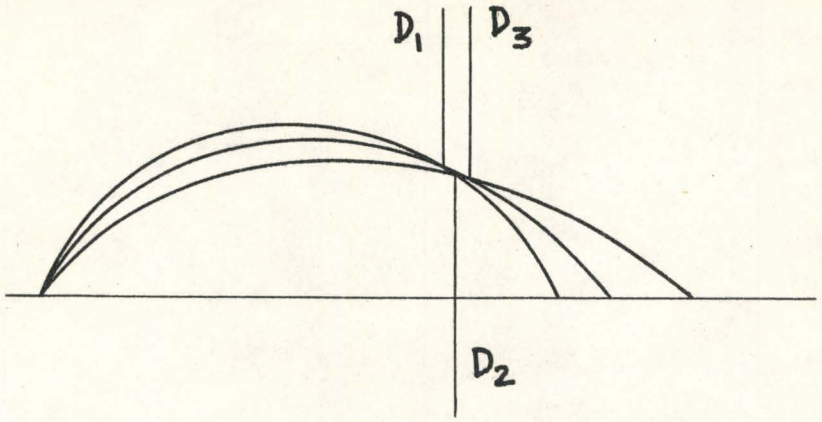

Figure 3

For the case of non-homogeneous fields where the electron trajectories cannot be calculated the shape and position of the ring focus can be determined using photographic film. The diaphragms D_2 and D_3 can be replaced by a single conical baffle and D_2 by a movable baffle. The gap between the movable and conical baffles then defines both the transmission and resolution of the instrument. One of the advantages of this system over the one proposed by Du Mond is that only the movable baffle D_2 is required to be adjusted to vary the transmission and resolution of the instrument, whereas in his instrument D_3 and D_4 must be adjusted for each setting of D_1 and D_2. The Hubert baffle is used in the Gerholm instrument.

(iv) Response of Spectrometer to a Monoergic Beam

The resolution $\frac{\Delta p}{p}$ defined above is a useful concept for many purposes but it is not as convenient for making quantitative deductions as the quantity η to be defined in this section.

To describe the response of a spectrometer to a monoergic electron beam of finite angular spread emerging from a source of finite area,

following Gerholm (32) we introduce the function $g(\xi, p)$ which is the probability of recording an electron of momentum ξ when the instrument is set to focus electrons of momentum p. If $\xi = p$ the value of g is unity. It can be shown that $g(\xi, p)$ is independent of p and depends only on $(\xi - p)/p$. Hence, writing $(\xi - p)/p = u$, we have $\int_0^\infty g(\xi, p)\, d\xi = p \int_{-1}^\infty g(u)\, du = p\eta$, where η is a constant for a given spectrometer and depends only on the source, detector and baffle geometry.

If a monoergic source of electrons of intensity $N(\xi_0)$ is placed in the spectrometer, the detector counting rate N (p) at an arbitrary value of p is $N(p) = N(\xi_0)\, \omega\, g(\xi_0 p)$ and the peak counting rate is $N(\xi_0)\omega$. If we now plot N/p vs p the area under the peak is

$$\int_0^\infty \frac{N(p)}{p}\, dp = \omega N(\xi_0) \int_0^\infty \frac{g(\xi_0 p)}{p}\, dp$$

However, since $g(\xi, p)$ vanishes unless $p \cong \xi_0$, the effective range of integration is so small that we can remove p from under the integral sign. Hence

$$\int_0^\infty \frac{N(p)}{p}\, dp = \frac{\omega N(\xi_0)}{p} \int_0^\infty g(\xi p)\, dp$$

$$= \omega N(\xi_0)\, \eta .$$

Thus η represents the area of the peak divided by the peak counting rate. In spectrometers where the peak profile is symmetric, η will be very nearly equal to the resolution $\Delta p/p$ defined earlier. This condition is satisfied for the Gerholm instrument with the Hubert baffle system. (See section vi.)

(v) Response of Spectrometer to a Continuous Distribution

For a beam of electrons of continuous energy distribution we

introduce a shape factor $\phi(\xi)$ which is the probability per electron, that the momentum will lie in a unit interval of momentum about ξ,

$\int_0^{N_0} \phi(\xi) d\xi = N_0$ where N_0 is the total number of electrons. When the spectrometer is set at p, the counting rate is

$$\int_0^{\infty} N \phi(\xi) g(\xi, p) \omega \, d\xi$$

In beta ray spectra $\phi(\xi)$ is a slowly varying function of ξ, compared to g. We may put $\phi(\xi) = \phi(p)$ = constant over the range of integration, and the counting rate becomes

$$N_0 \phi(p) \eta p \omega$$

If $\frac{N}{p}$ is plotted against p, the area under the curve is given by

$$\int_0^{\infty} \frac{N}{p} dp = \int_0^{\infty} \frac{N_0 \phi(p) \eta p \omega \, dp}{p} = N_0 \eta \omega$$

The approximation that ϕ remains constant over the range of finite values of g is valid in most practical cases. A large resolution can, however lead to errors in the determinations of areas, and end points of beta spectra of the order of a few percent.

(vi) Theory of the Triangular Field Spectrometer

The focussing conditions for a lens spectrometer are difficult to treat mathematically and complete theories exist for only two types, the thin lens and the homogeneous field lens. For other cases it has often proven more advantageous to carry out experimental explorations of the focussing properties. In the Gerholm (24) instrument, H_Z on the symmetry axis is zero at the source position and increases roughly linearly with z as one moves towards the detector. Gerholm (24) had shown the advantages of such a field form but no theoretical treatment of its properties was available until the present instrument

was well under construction. In 1957 and 1958 two papers dealing with this topic appeared. Lindgren (33) discussed the performance of a pure triangular field and showed that the maximum luminosity was superior to that of a uniform field. A shape between a triangular and uniform one, however, would be even better. Ramberg and Blaugrund (34) dealt with such a field shape. Their paper is useful in deducing the general focussing properties of the Gerholm instrument but not of much value in locating the actual baffle positions. Some discussion of their theory and comparison of its predictions with the results obtained from the McMaster lens seems waranted. Curve (a) of Figure 5 presents the measured value of B_z on the symmetry axis as a function of z for the McMaster instrument with a coil current of 20 amperes. The field shape was determined for various current values and found to be independent of this parameter as expected. The lower part of the figure also shows the location of the source ring focus and detector.

Ramberg and Blaugrund dealt with a simpler field than this one. They considered the focussing effect of a field rising uniformly along the symmetry axis (i.e. $B_z = Kz$) up to a position Z_0 and then becoming constant

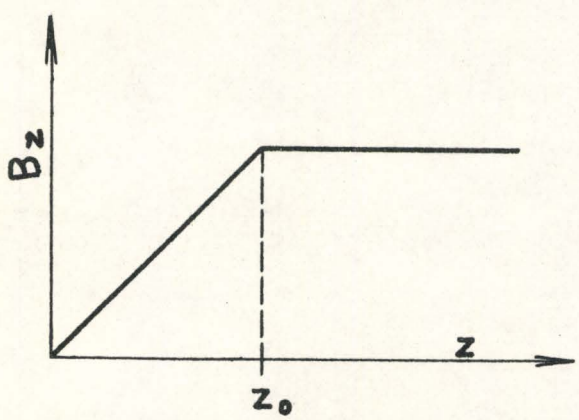

Figure 4

The equations of motion of an electron in the linearly rising portion of this field are $\ddot{r} = -(\frac{K}{2m})^2 z^2 r$, $\ddot{z} = -(\frac{K}{2m})^2 r^2 z$, where r is the distance from the symmetry axis and z is the distance measured from the source along this axis. If we define $\rho = \frac{r}{R}$ and $\zeta = \frac{z}{R}$ where $R^2 = \frac{2B\rho}{K}$ and $B\rho$ is the electron momentum, the equation of the path is given by:

$$\rho''(1-\rho^2\zeta^2) = \rho\zeta(\rho\rho' - \zeta)(1+\rho'^2)$$

The solution is of the form $\rho = \sum a_n \zeta^n$ where the a_n are specified functions of tan α the angle of emission of the electron from the source. Beyond the point where the field becomes constant, the electron trajectories are difficult to calculate analytically. Ramberg and Blaugrund (34) give the results for computer calculations for $\alpha = 26.5^\circ$ and 31.0°. They describe these results in terms of the following parameters:

Z_o, the position where the field becomes uniform

D, the maximum value of r

Z_ζ and Z_r, the coordinates of the ring focus and $(2\Delta p/p)/T^2 \equiv A$

Graphs are presented for $A, r_{f/D}$ $Z_{f/D}$ as a function of $Z_{o/D}$. We may compare the predictions of this theory with the performance of the McMaster Instrument. For this instrument $\alpha = 30^\circ$ and hence $\rho = 0.577\zeta - 0.0256\zeta^5 - 0.0022\zeta^9 - 0.00025\zeta^{13}$ The maximum value of ρ occurs at $\zeta = 1.3$. From the dimensions of the vacuum chamber, $D \sim 6.2$ cm so that R = 10.0 cm. This enables us to plot the trajectory up to $Z = Z_o$ (see curve (b) of Figure 5).

Since $K = \frac{2B\rho}{R^2}$, one can immediately determine its value from the fact that the electron momentum focussed, for I = 20 amperes, is 14,900 gauss-cm.

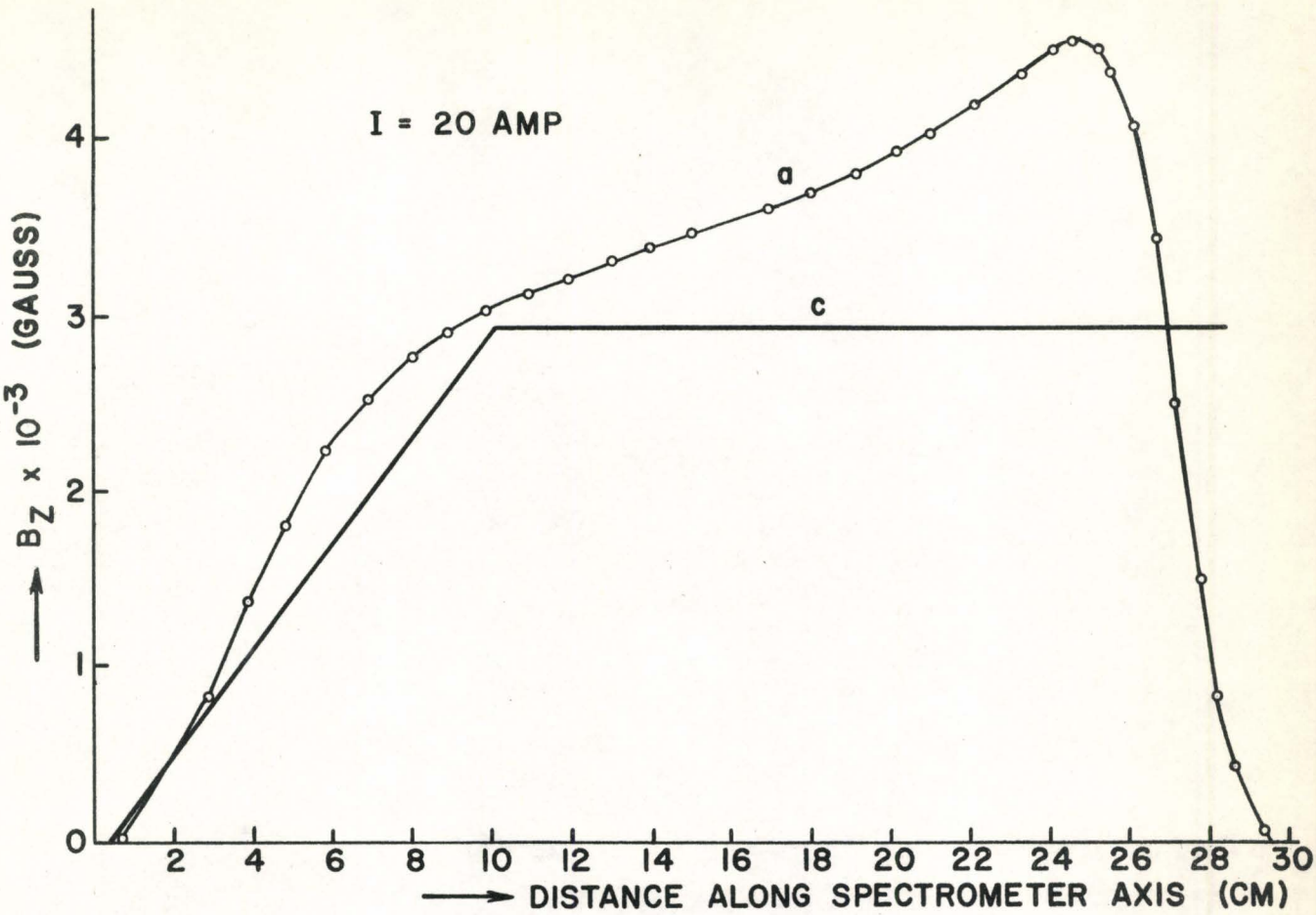
I = 20 AMP
a
c
$B_Z \times 10^{-3}$ (GAUSS)
0
1
2
3
4
2 4 6 8 10 12 14 16 18 20 22 24 26 28 30
DISTANCE ALONG SPECTROMETER AXIS (CM)

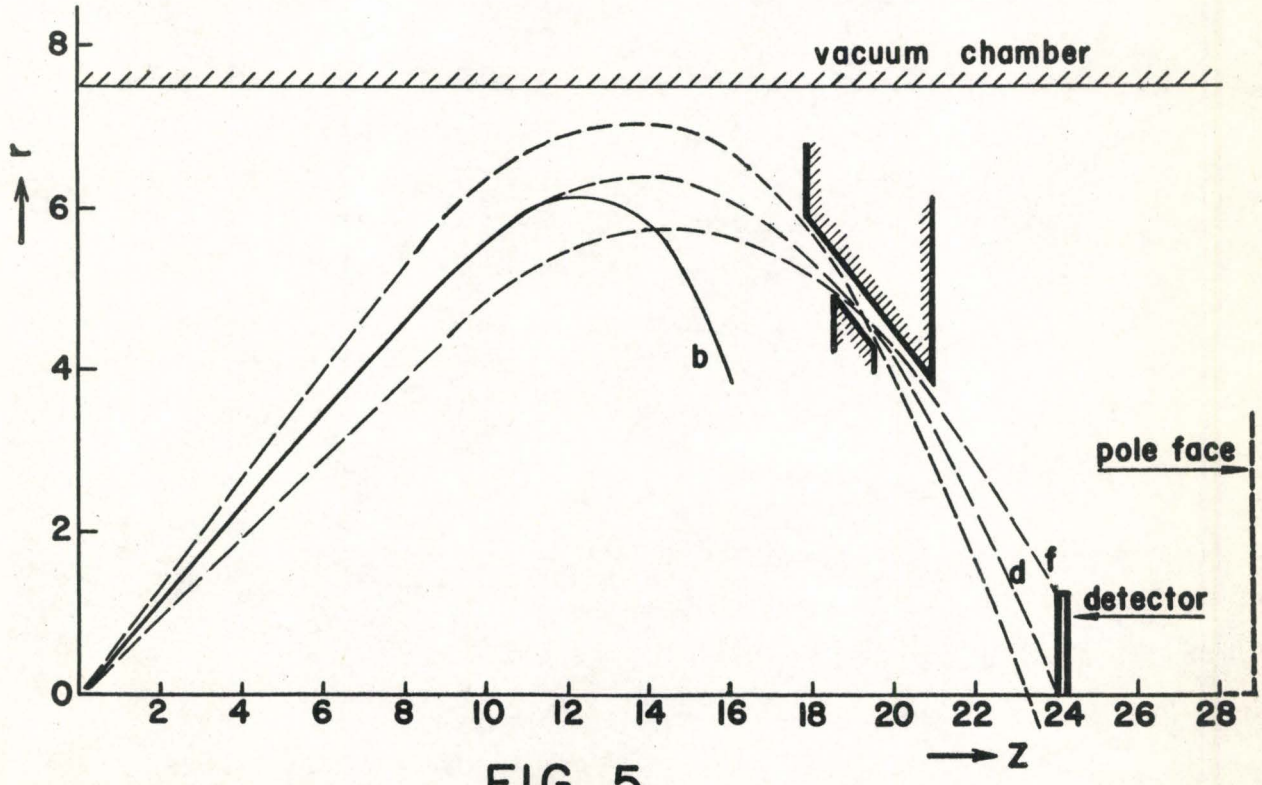
vacuum chamber
r
0
2
4
6
8
b
d
f
pole face
detector
2 4 6 8 10 12 14 16 18 20 22 24 26 28
Z

FIG. 5

The necessary value of $Z_o = 9.3$ cm for this field can be deduced from Ramberg and Blaugrund's paper using the datum A = 21. This idealized field curve c of figure 1, shows a broad similarity to the actual field although one would have hoped for a larger value for Z_o. The coordinates of the ring focus for the idealized field are $z_f = 19.3$ cm and $r_f = 4.7$ cm, in excellent agreement with the observed values at 19.5 and 4.4 cm respectively. The lower part of Figure 5 shows the ray at 31.0^o drawn to pass through the ring focus. The expected paths of two extreme rays on either side of it are also shown.

CHAPTER III

THE THEORY OF COINCIDENCE COUNTING

(i) Introduction

An electron-electron coincidence spectrometer is designed to study coincidences between conversion electrons on the one hand and decay electrons or conversion electrons on the other, i.e. e-β or e-e coincidences. In addition, by removing the baffles from one spectrometer and inserting a Sodium Iodide (Tl activated) crystal scintillation spectrometer β - γ and e-γ coincidences may be studied. Equipment for this latter type of experiment was built and tested but was not used in the Os^{193} investigation and will not be discussed further here.

It will be assumed in the following discussion that a suitable source mounted on a thin backing has been placed in the spectrometer so that electrons can pass freely into both focussing fields, and that the coincidence circuit has been set up to record coincident events from the two detectors with 100% efficiency. Under these conditions we shall examine the information which may be obtained from e-β and e-e coincidence experiments.

(ii) e-β Coincidences

In these experiments, one spectrometer is set on the peak of a conversion line while the other one scans the continuum. The coincidence counting rate yields the spectrum of beta rays in coincidence with the conversion line and this

spectrum can be subjected to Fermi analysis in the usual way. A linear Fermi plot will indicate a simple beta spectrum (assuming an allowed shape) while departure from a straight line will indicate the presence of two or more partial spectra in coincidence with the conversion electron. The situation is illustrated in the figure 6.

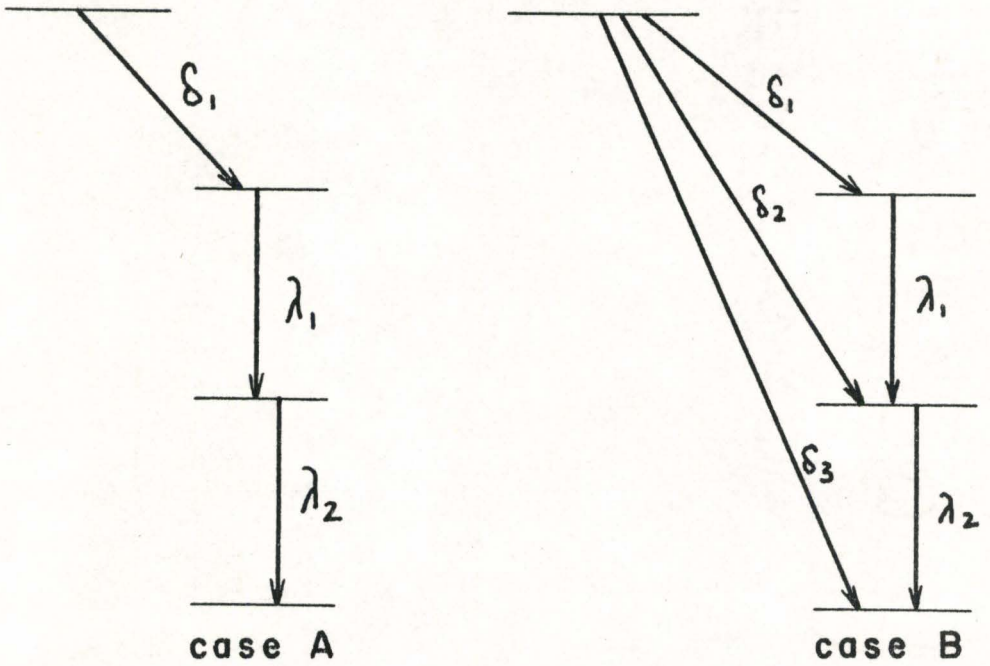

Figure 6

For case A the coincidence spectrum with spectrometer No 1 on λ_1, will have the same end-point (but not the same intensity) as that obtained when it is set on λ_2. In case B, the coincidence spectrum with spectrometer No 1 on λ_2, will yield two spectra δ_1 and δ_2 under Fermi analysis. The difference in the end-point of δ_1 and δ_2 will be equal to λ_1 and the difference in the end-points of δ_2 and δ_3 (if this is known) will be equal to λ_2. This type of experiment breaks up the initial complex spectrum into simpler components which are more easily analyzed. The

area under the coincidence spectrum when combined with the area under the single channel spectrum will yield the branching ratio or the conversion probability (of the beta group or the conversion electron respectively) depending on which one of these is known.

Let us consider the simple case of a beta spectrum of intensity δ_1 feeding a level which decays by a transition λ_1 figure 7.

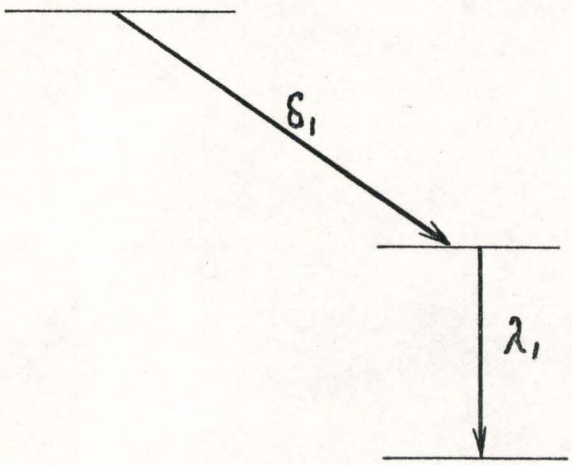

Figure 7

Suppose that spectrometer No 1 is set to focus a conversion line of momentum p_1 and spectrometer No 2 is set to focus beta rays of momentum p_2 from the continuum. The single channel counting rates will be

$$N_1 = N_0 \phi(p_1) \omega_1 \eta_1 p_1 + N_0 \delta_1 \kappa \omega_1$$

$$N_2 = N_0 \phi(p_2) \omega_2 \eta_2 p_2$$

where the symbols have the same meaning as in Chapter II. Of the events recorded in spectrometer No. 2, a certain number belong to the partial spectrum δ_1 which lead to the transition λ_1. These are No $\delta_1 \phi_{\delta_1}(p_2) \omega_2 \eta_2 p_2$ where $\phi_{\delta_1}(p_2)$

is the shape factor of the partial spectrum δ_1 such that

$$\int N_0 \delta_1 \phi(E)\, dE = N_0 \delta_1$$

Of these events the fraction registered in spectrometer No 1 is $\omega_1 \kappa_1$. The coincidence counting rate is therefore $N_0 \delta_1 \phi_1(p_2)\, \omega_2 \eta_2 p_2\, \omega_1 \kappa_1 = N_c$

The area under the curve $\frac{N_c}{p}$ versus p is

$$\int \frac{N_0 \delta_1 \phi_{\delta_1}(p_2)\, \omega_2 \eta_2\, p_2\, \omega_1 \kappa_1\, dp_2}{p_2} = N_0 \delta_1 \omega_1 \omega_2 \eta_2 \kappa_1$$

If we combine this with the area under the singles curve Chapter II (v), we get

$$\int_{co} \frac{N(p)}{p}\, dp \Big/ \int_{s} \frac{N(p)}{p}\, dp = \frac{N_0 \delta_1 \omega_2 \eta_2 p_2\, \omega_1 \kappa_1}{N_0 \eta_2 \omega_2} = \delta_1 \omega_1 \kappa_1.$$

The solid angle ω_1 can be measured readily and so if either δ or κ is known, the other may be found. The product $\delta\kappa$ is simply the number of conversion electrons per disintegration. If the level formed by the transition δ_1 decays by another mode in addition to λ_1, then the coincidence counting rate will be reduced by a factor equal to the branching ratio for transitions from this level.

(iii) e - e Coincidences

In e - e coincidence experiments one spectrometer is focussed on one peak while the other spectrometer scans the other peak. Since both conversion lines are in coincidence with partial beta continua the profile of line 2 which is scanned while line 1 is fixed is due to coincidences of line 2 with line 1 and with partial spectra. The contribution due to the continuum must then be determined by moving the first spectrometer off line 1 and re-scanning line 2. The difference between the two peak heights so obtained is then the coincidence rate due to line 1 and line 2 coincidences. In some cases, particularly when the transitions are weakly converted, the signal to noise ratio may be very poor and obtaining data

with statistical significance can be very difficult. Apart from revealing the "generic" relationships between transitions, e - e coincidences can, in favourable cases, give conversion probabilities directly.

By arguments similar to those in the last section one can show that the coincidence counting rate due to two transitions λ_1 and λ_2 is:

$$N(\lambda_1 \lambda_2) = N_0 \delta_1 \omega_1 \kappa_1 \omega_2 \kappa_2$$

where δ_1 is the total probability for transition λ_1. Since the single channel peak height is $N(\lambda_1) = N_0 \delta_1 \kappa_1 \omega_1$,

$$N(\lambda_1 \lambda_2) / N(\lambda_1) = \frac{N_0 \delta_1 \kappa_1 \omega_1 \omega_2 \kappa_2}{N_0 \delta_1 \omega_1 \kappa_1} = \omega_2 \kappa_2.$$

This ratio gives the conversion probability κ_2 directly since ω_2 is measurable in the spectrometer. Here again if λ_2 is not the only transition possible from that level, the coincidence counting rate will be reduced by a factor equal to the branching ratio. The observed coincidence counting rate when both spectrometers are focussing the conversion peaks λ_1 and λ_2 is due to $(\lambda_1 \beta) + (\lambda_2 \beta) + (\lambda_1 \lambda_2)$. The contributions from $(\lambda_1 \beta)$ and $(\lambda_2 \beta)$ coincidences constitute unwanted or noise counts and must be deducted to get the true rate. In practice, the whole profile of the peak need not be scanned in the coincidence spectrum unless there are interfering lines close to it. The counting rates "on" and "off" the peaks may be used to get the various combinations of $(\lambda_1 \beta)$, $(\lambda_2 \beta)$ and $(\lambda_1 \lambda_2)$ coincidences. The coincidence counting rates are

$$N(\lambda_1 \beta) = N_0 \delta_1 \kappa_1 \phi_1(p) \omega_1 \omega_2 \eta_2 p_2 \,, \quad N(\lambda_1 \beta) = N_0 \delta_2 \phi_2(p) \kappa_2 \omega_2 \omega_1 \eta_1 p_1$$

where $\phi_1(p)$ and $\phi_2(p)$ are the shape factors for the beta spectra associated with λ_1 and λ_2 respectively. The signal to noise ratio is therefore:

$$\frac{N(\lambda_1\lambda_2)}{N\{(\lambda_1\beta)+\lambda_1\beta)\}} = \frac{N_0\,\delta_1\,\omega_1\,\varkappa_1\,\omega_2\,\varkappa_2}{N_0\,\delta_1\,\omega_1\,\varkappa_1\,\phi_1(p)\,\omega_2\,\eta_2\,P_2 + N_0\,\delta_2\,\omega_2\,\varkappa_2\,\phi_2(p)\,\omega_1\,\eta_1\,P_1}$$

$$= \frac{\delta_1\,\varkappa_1\,\varkappa_2}{\delta_1\,\varkappa_1\,(\phi_1(p)\,\eta_2\,P_2) + \delta_2\,\varkappa_2\,(\phi_2(p)\,\eta_1\,P_1)}$$

Obviously one can improve the signal to noise ratio by keeping the resolution η of each spectrometer as small as possible. It is difficult to decide beforehand whether a certain coincidence combination will give a good signal to noise ratio or not unless a good deal is known about the decay scheme in question. In general, one might say that e - e coincidence experiments are favoured in cases where the conversion electrons are situated on a very low back ground (e.g. K capture, or conversion electrons beyond or near the beta end-point.) Conversion electron-beta continuum experiments on the other hand generally give a high signal to noise ratio, since the only noise present is due to scattering in the spectrometer itself. The counting rates in these experiments can be made large by using large values of η and ω. In such cases large sources may be used to advantage, whereas for e - e coincidences, small sources are preferable.

It should be finally noted that if both e_1 - e_2 and e_1 - β coincidences can be studied from the same source, the ratios $\omega_1\,\varkappa_1$ and $\delta_1\,\omega_1\,\varkappa_1$ will yield δ directly without any necessity of determining ω or $\varkappa_1$.

CHAPTER IV

THE ELECTRON-ELECTRON COINCIDENCE SPECTROMETER

(i) Introduction

The two halves of an electron-electron coincidence spectrometer should be magnetically independent of each other, or awkward problems of correcting for the effects of the stray field of one on the focussing properties of the other would have to be overcome. Most thick lens spectrometers operate with the source within the magnetic field region. If a single source is to be used with two different lenses their magnetic fields should not overlap, and so, it is best to employ lenses with their magnetic fields dropping to zero at the source. This field form has been discussed in Chapter II, section v. It is capable of better performance than the homogeneous field, since larger sources can be used under the same conditions of transmission and resolution. An approximately triangular field shape may be realized in a long solenoid with pole pieces at the extremities as shown in Figure 8. The pole piece at the source end is receding from the field region and the pole piece at the detector end is bulging into the field. The outer iron yoke provides a low reluctance path for the magnetic flux outside the solenoid. Both solenoids may be placed in the same iron yoke with a single centre pole piece common to both instruments. The outer pole piece may be a composite unit, half of it serving as a pole piece for one spectrometer and half of it for the other. The source position is then at the pole piece and electrons enter both spectrometers

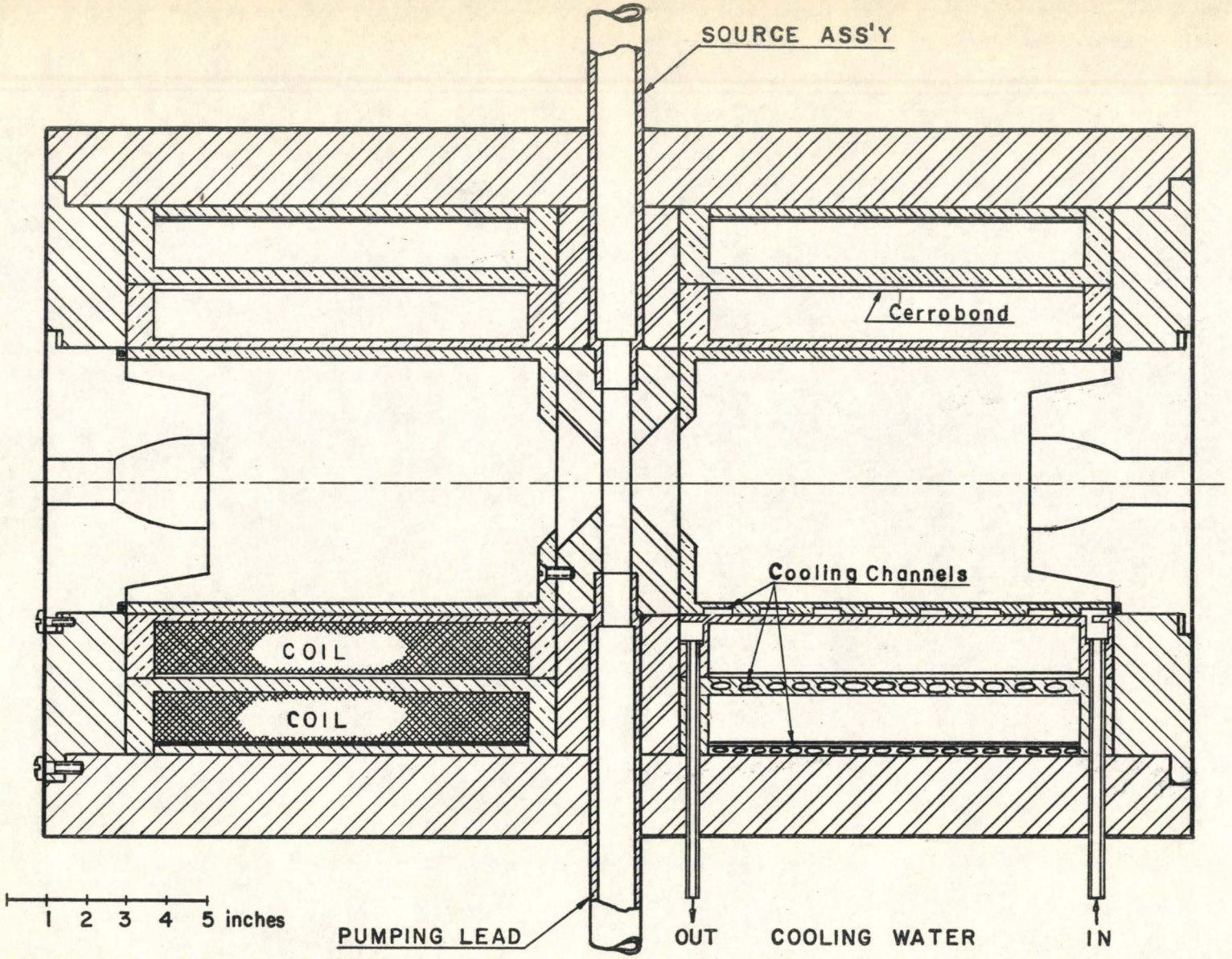

FIG.8 COINCIDENCE SPECTROMETER

via openings in it. The axis of symmetry of the iron yoke is the common axis for both the pole pieces and the magnetic coils.

(ii) Physical Dimensions and Power Requirements

A sectional drawing of the spectrometer is shown in figure 8. Its geometrical shape is that of a hollow cylinder of Armco iron with walls 2" thick. The ends of the cylinder are closed with flanges of the same thickness and the centre portion is nearly closed by a disc of 4" thickness. The total mass of the iron is approximately 800 lbs. The copper coils which fit inside the cylinder are four in number and have a total mass of about 800 lb. The two vacuum chambers are cylinders of diameter 6" and length 10". Most of the space in these chambers is filled with pole pieces, baffles and gamma ray shielding, not shown in the figure. The outer cylinder is pierced at various points to allow for the insertion of the light pipes, the source holder, the pumping lead and the electrical and water connections.

Gerholm's instrument required 60,000 ampere turns to focus 3.5 Mev electrons. The McMaster instrument has 3400 turns, is capable of handling 30 amperes and focussing 6 Mev electrons. However the power dissipation at this current is 9 kilowatts, considerably above the 5 kilowatt rating of the d. c. generators available. Within the limits imposed by the generators, the instrument can focus electrons up to 4.5 Mev .

(iii) The Magnet Coils

Since it was important for good focussing that the coils be axially symmetrical and possess uniform current density along their lengths, it was decided to wind

the coils on machined spools using square section wire (No. 12 AWG). The restricted space available for the coils and the high current density required made it necessary to use two concentric coils for each lens with water cooling at the outer and inner faces of each coil. With this design, the temperature at the centre of each coil does not rise above 80°C at 5 kw. Each inner coil, Figure 8, was wound on a spool which was machined to close tolerances to maintain cylindrical symmetry. The inner surfaces of the flanges were insulated with micarta, and the curved surface of the spool was covered with a glass and mica insulating fabric. During the winding operation a constant tension was maintained on the wire, and each turn was pressed alongside the previous one without leaving any visible gap. At the end of each row the "fly-over" was brought over smoothly to the next. Each row was covered with a very thin insulating plastic film. Each completed coil had 16 layers of 106 ± 1 turns per coil. The outer radius of the coil was measured at a large number of points along its length and at various azimuth angles. The deviations from axial symmetry were small and random with a r.m.s. value of 0.003". Each coil was then covered with a glass and mica fabric. The spool for each outer coil had a spiral groove cut in its curved surface, into which a copper tube for cooling water was soldered. The surface was then machined true, and the coil wound in the standard manner. The completed coils were then fitted together and tested. It was found that overheating of the inner coils occurred because of the poor heat transfer through the narrow air gap between the outer face of the inner coils and the inner face of the outer coils. The situation was remedied by pouring cerrobend (a Lead-Bismuth-Tin alloy which melts at 78°C) into the cavity.

The vacuum chambers were bronze cylinders with spiral grooves cut in their outer surfaces. These chambers fitted snugly into the inner spools and the interface at each end was sealed with O-rings. Thus the grooves on the vacuum chamber served as channels for the water required to cool the inner coils.

(iv) The Vacuum System and Source Holder

Vacuum tight seals were made between the chambers and the pole pieces by means of O-rings. The chambers were connected to the vacuum pumps by means of a pumping lead which was attached to the centre pole piece. With an oil diffusion pump and a small fore pump the system can be pumped down to less than 10^{-4} mm of Hg within ten minutes. The source holder shown in Figure 9 was designed to allow the source to be inserted into, or withdrawn from the spectrometer without disturbing the vacuum. It consists of a set of tubular sections with O-ring seals between them. The source is mounted on the innermost tube. Its position on this tube is adjusted in a specially made jig so that when inserted in the spectrometer it will be located on the mid point of the axis of symmetry.

(v) The Pole Piece and Detectors

The pole piece and the detector assembly at the detector end of the instrument are shown in Figure 10. No attempts were made to vary the profiles of either pole face since the first set used gave good performance. The opening through the pole piece was designed to be used with the Gerholm light pipe described below.

An anthracene, or plastic scintillator was placed at S to detect the electrons. It is essential that an efficient method be provided to transmit the

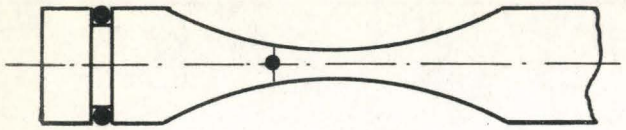

PART B

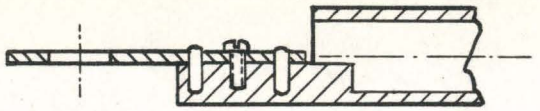

PART C

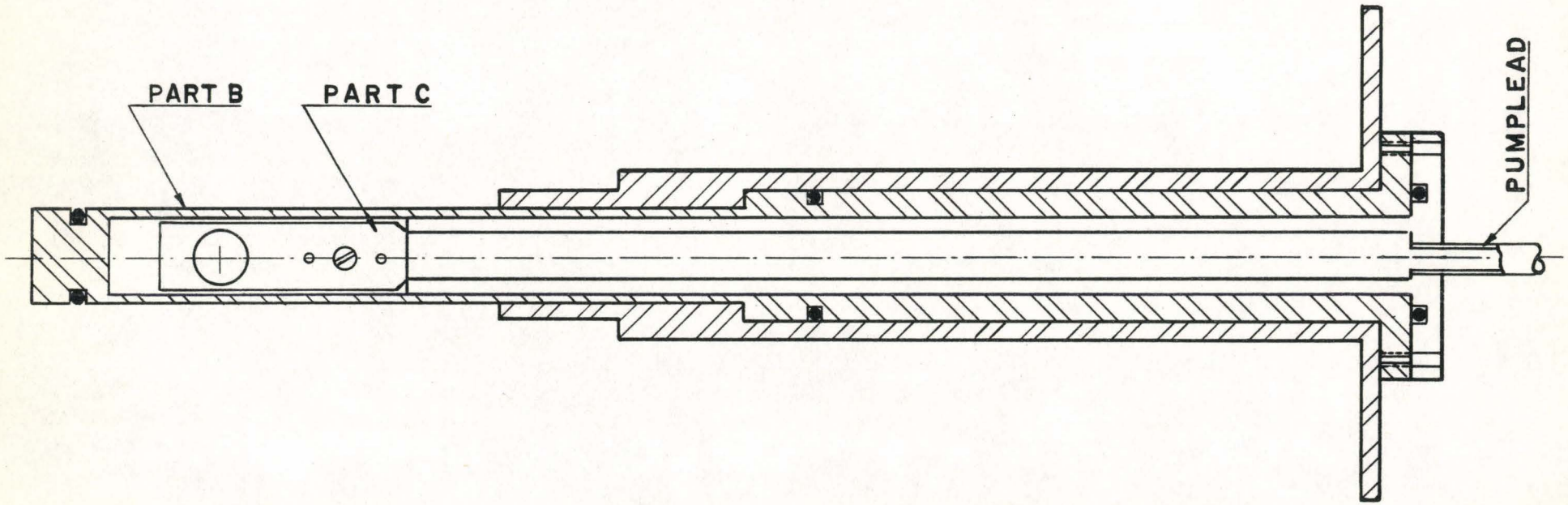

FIG. 9 SOURCE HOLDER

DETAIL B and C Viewing 90° rotated

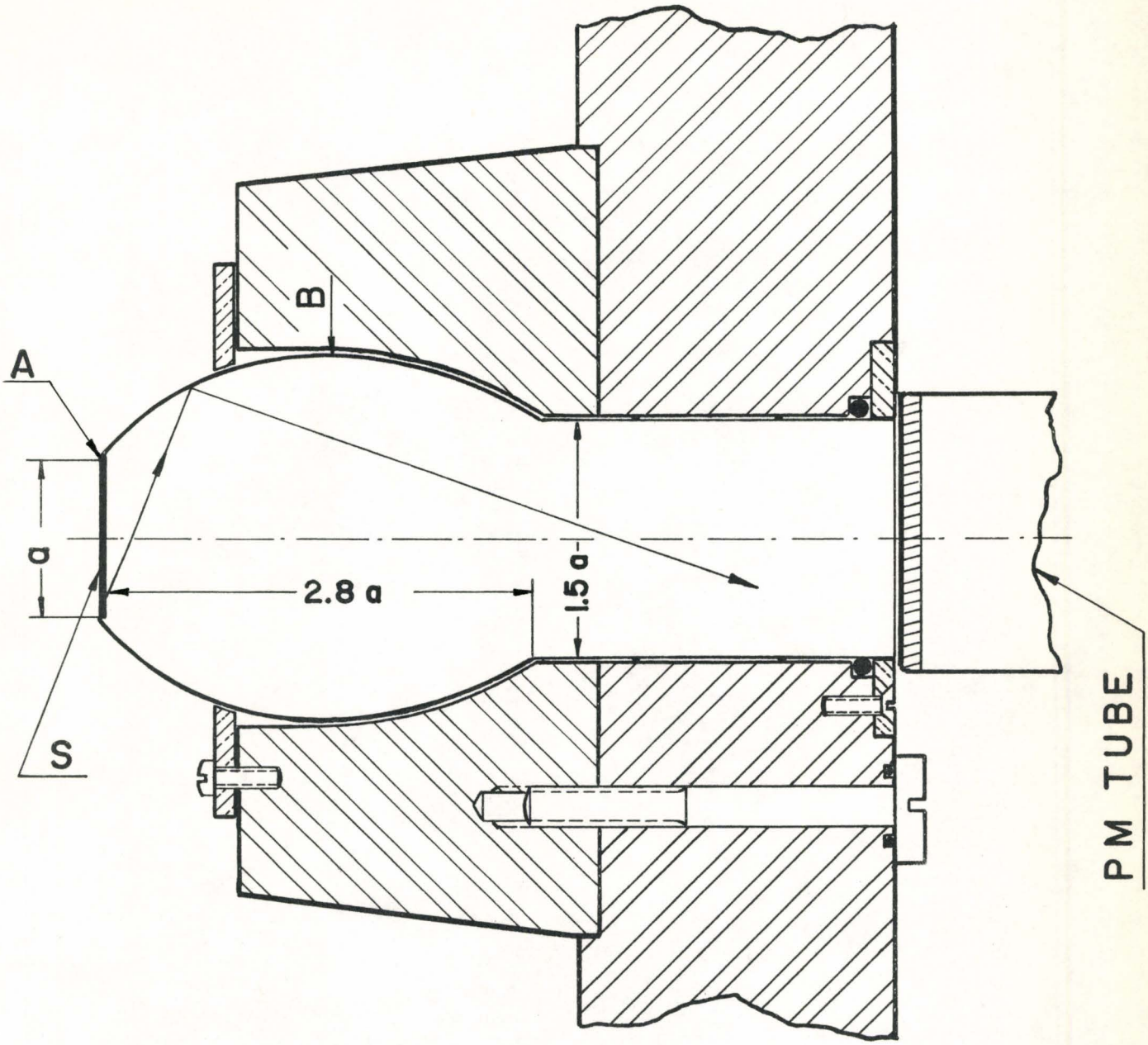

FIG. 10

DETAIL OF DETECTOR AND LIGHT PIPE

scintillator light output to the photomultiplier. An ordinary cylindrical light pipe will not transmit more than one-third of this output. The pipe shown in the figure will deliver almost all the light thrown into the forward cone. When a thin aluminium reflector was placed over S, the light transmitted was increased by about 30%. The profile of the light pipe from A to B is a logarithmic spiral of the form $R = a \exp(\theta \tan c)$ where c is the critical angle and a is the diameter of the detector. For lucite, with index of refraction equal to 1.501, this pipe will reach a maximum diameter of 1.86 a at a distance 1.277 a from S. If the profile is made to follow the spiral beyond B second reflections will meet this surface at less than the critical angle. If the spiral is abandoned at B and the profile continued as a cylinder of diameter 1.86 a, all higher order reflections will meet the surface at angles greater than the critical angle. However, it is still possible to reduce the diameter of the pipe gradually, reaching a value 1.50 a at a distance 2.80 a without losing any more light. Beyond this point the pipe must be continued as a cylinder of diameter 1.50 a. This second choice has the advantage of requiring a smaller hole in the pole piece and a smaller photomultiplier.

(vi) Spectrometer Power Supply

(a) Schematic Diagram

A block diagram of the power supply is shown in Figure 11. The output of the 5 kilowatt generator is filtered by means of a standard L C filter to reduce the value of the commutator ripple and applied to the magnet coil in series with a standard resistor. The voltage developed across this resistor and a reference voltage are both applied to a difference amplifier. The amplified difference signal is then

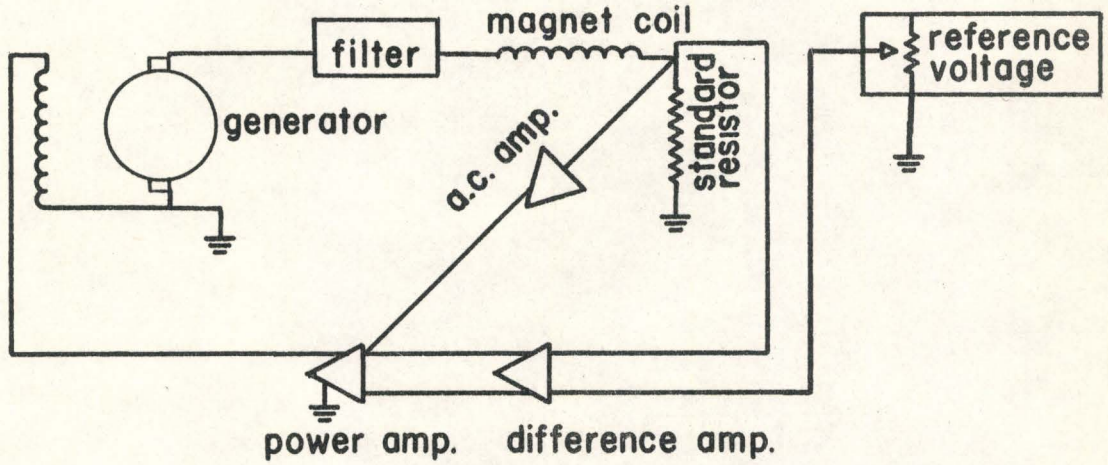

Figure 11.

fed to a power amplifier which alters the current to the field coils of the generator in such a way as to reduce the difference voltage to zero. In addition, an a c amplifier is connected as shown to prevent the circuit from "hunting". The magnet current may be set at any predetermined value by adjusting the reference voltage. The short term stability of this stabilizer was about one part in 5000, a value quite sufficient for the needs of the experiment. The long term stability (i. e. over a period of weeks) was about one part in 2000. Each part of this circuit will be discussed in turn.

(b) The Standard Resistors

The standard resistors are made of constantan ribbon wound on a brass pipe and insulated from it by two layers of baked Formel enamel. This pipe is included in the cooling system for the magnet and is thus kept at the temperature

of the city water mains. Each resistor is fitted with current and potential leads as shown in the sketch, Figure 12. Under these conditions of operation, the largest change in current due to temperature changes in the resistors is less than one part in 20,000.

(c) The Reference Voltage

The continuously adjustable reference voltage is provided in the circuit of Figure 12. Since its effectiveness depends on the properties of the 5651 voltage reference tubes, some efforts were made to examine their long and short term stability. It was found that these tubes were stable to about one part in 10,000 over periods of a few hours. However they are subject to occasional sudden changes which might be as large as one part in 2,000. Even with this limitation these tubes seem to be adequate as standards for an instrument whose resolution was one or two percent.

Since the reluctance of the magnetic path is dominated by the air gap, the field produced in the spectrometer and hence the momentum of the focussed electrons varies linearly with current. The reference voltage however is proportional to this current so that the helipot setting is a linear function of momentum. On each range the momentum focussed can be varied by a factor of two, and it was a simple matter to inter-calibrate the ranges.

(d) The Difference Amplifier

The difference amplifier, a four terminal device, is presented in detail in Figure 13. Its chopper converts the difference of the two input voltages into a square wave which is amplified by an a. c. amplifier and detected by a phase sensitive detector. The phase of the a. c. signal is reversed when the sign of the

difference voltage is reversed. The a.c. amplifier consists of three push-pull stages with current feed-back via cathode resistors on each stage and a gain which is variable from zero to a maximum of 180,000. At full gain, an input of 300 μvolts is sufficient to overload the amplifer. It is therefore of paramount importance to keep the ripple voltage into the chopper at a very low level. The phase sensitive detector is in effect two full-wave rectifier circuits employing 6SN7 twin triodes. Two transformers apply sixty cycle per second signals between the grids and cathodes of these tubes. One rectifier gives a positive output voltage and the other a negative output voltage and these are made conducting alternately. An incoming a.c. signal is rectified to give a positive or a negative output depending on its phase with respect to the switching of these rectifiers. The difference amplifier therefore gives an output voltage which depends on the sign and magnitude of the difference between the two input voltages.

(e) The Power Amplifier

The power amplifier, Figure 12 consists of one voltage amplifier stage and six 6AS7G tubes in parallel. The generator field coil forms the cathode load for these tubes.

The power supplies for the difference amplifier and the power amplifier are shown in Figure 14. They are of conventional design and need no comment.

(f) The Filter

The ripple frequencies present in the output of the generator are 50 c/s, 100c/s, 400c/s, and other frequencies up to 1.8kc/s. The resistance of the magnet coil is ten ohms and the inductance 0.29 henry, so that the attenuation

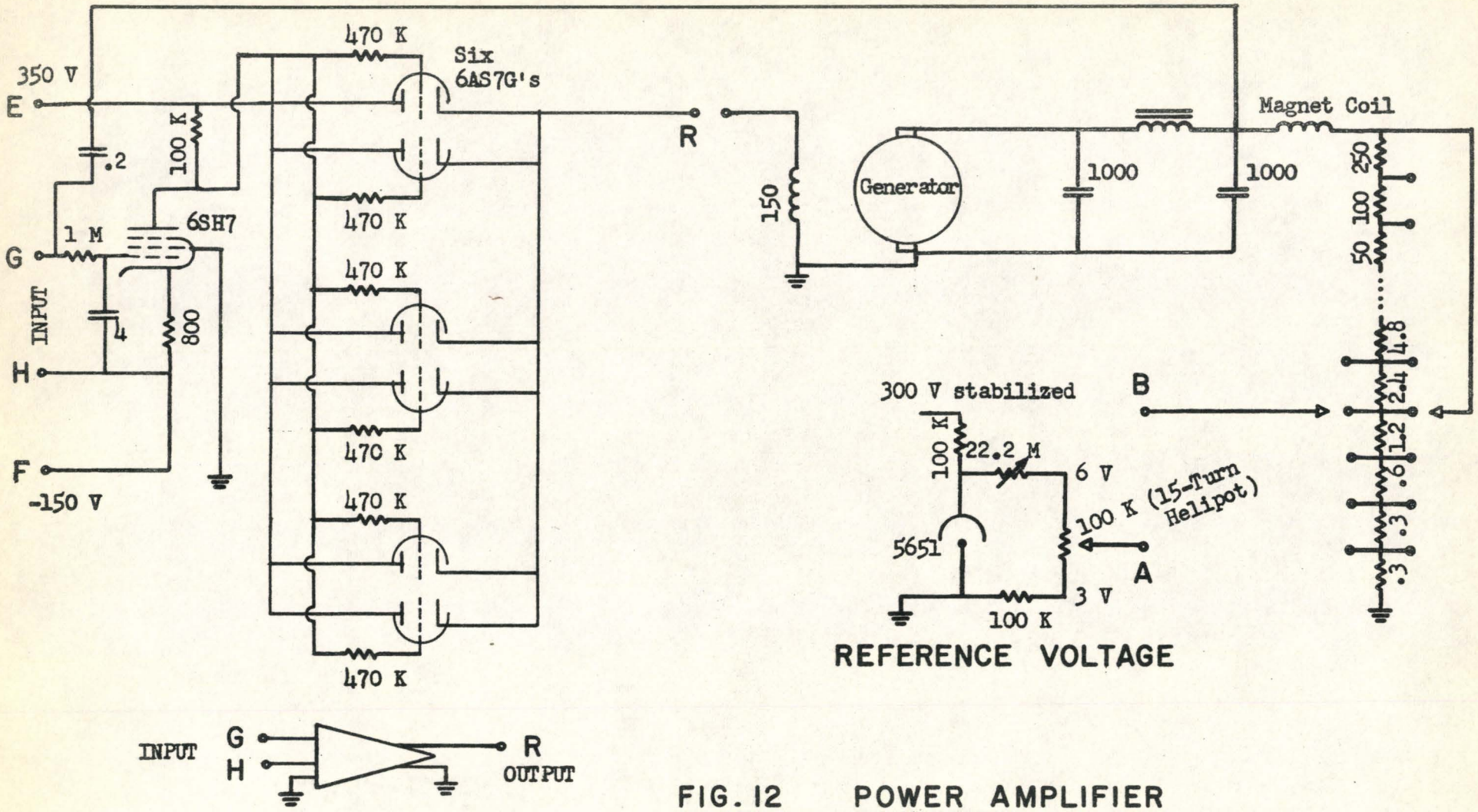

FIG. 12 POWER AMPLIFIER

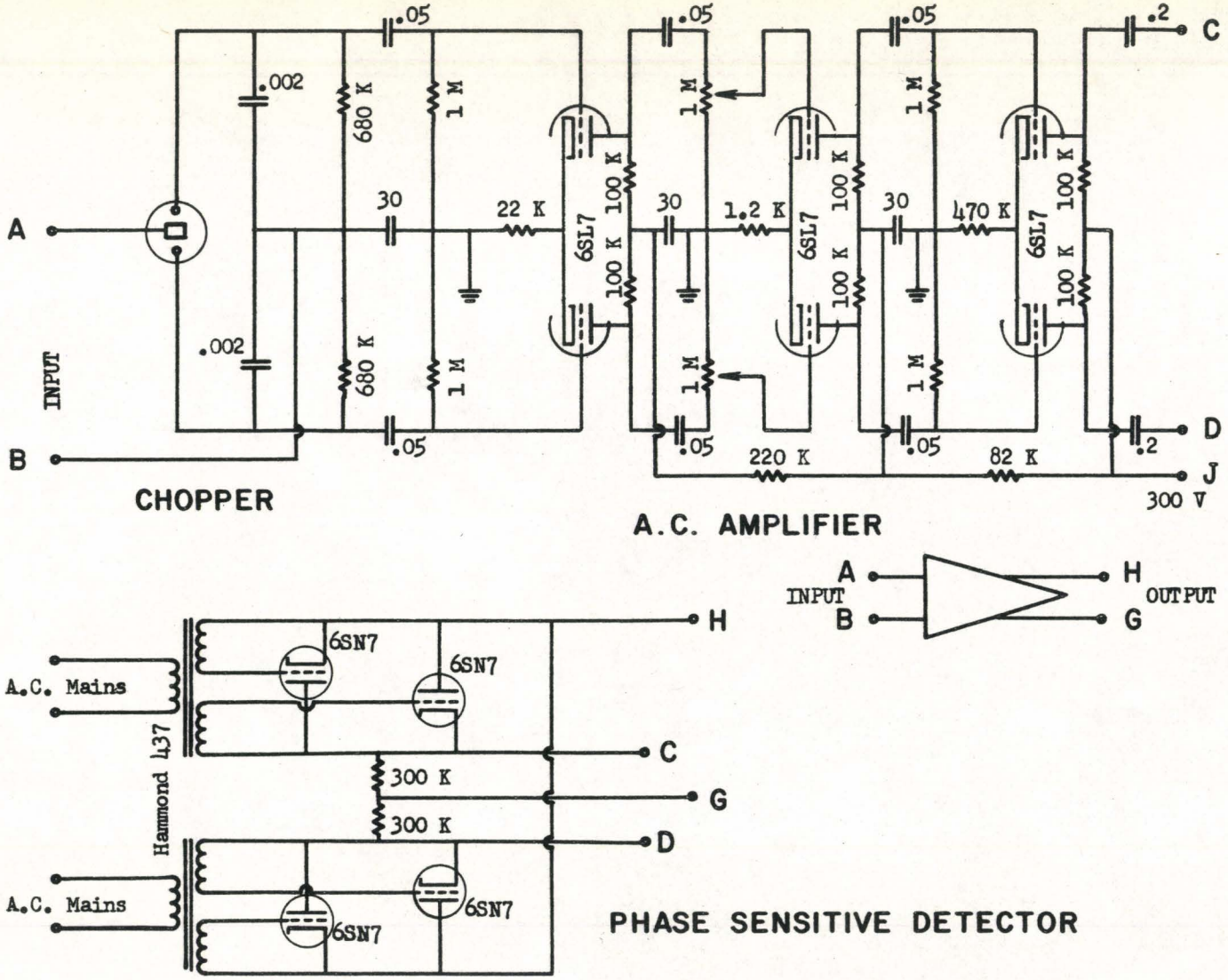

FIG. 13 DIFFERENCE AMPLIFIER

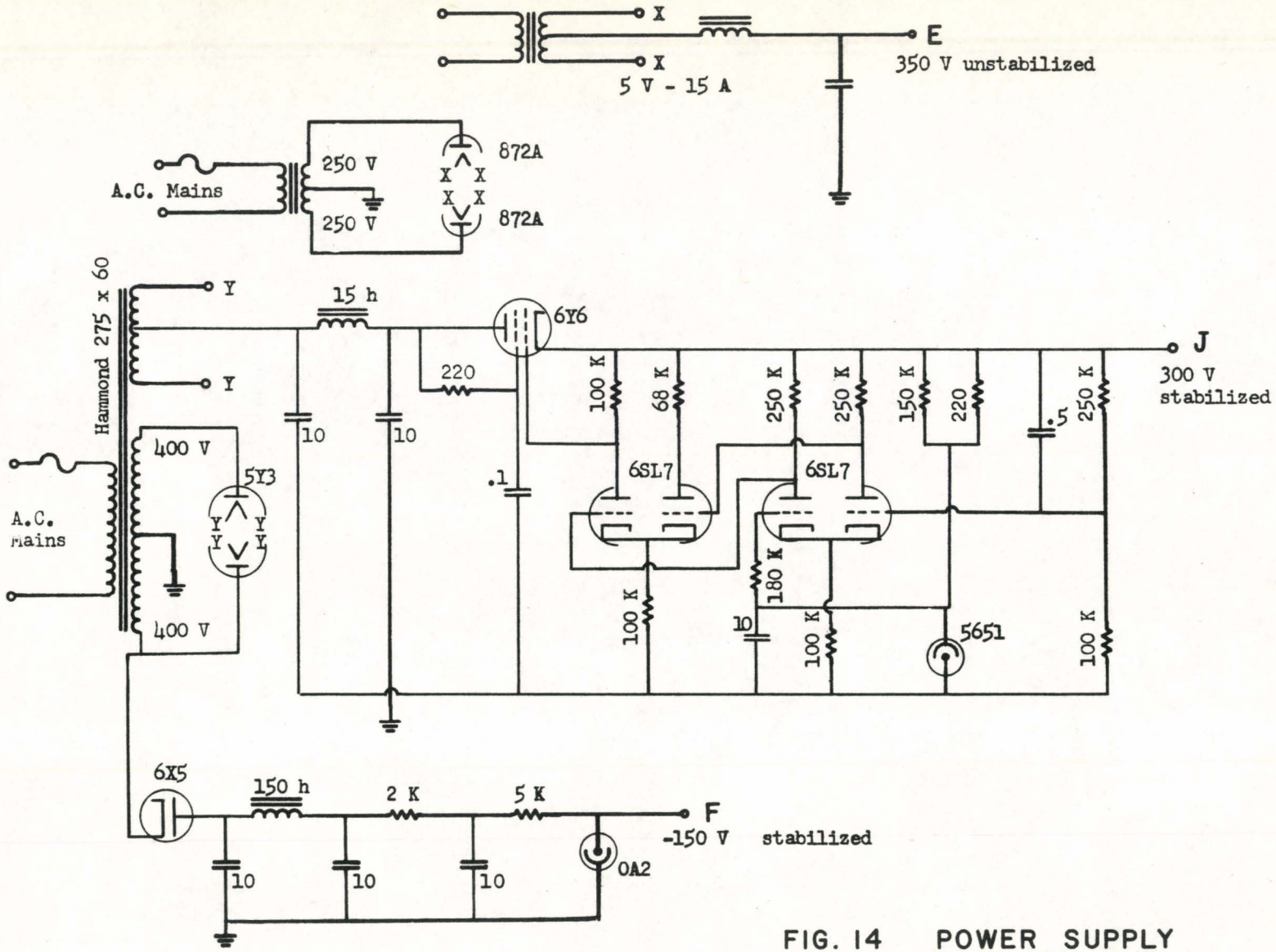

FIG. 14 POWER SUPPLY

of the low frequency components by the magnet is not very great. It was quite unrealistic to remove these frequency components by an a. c. feedback loop through the generator field coils since the upper frequency cut-off of the generator is close to sixty cycles per second. The simplest solution was to use a LC filter consisting of a twenty ampere variac and two banks of electrolytic condensers of 1000μF each. This filter reduces the ripple current at 50c/s to about one part in 5, 000 of the direct current. The ripple currents at higher frequencies are considerably smaller. This filtering was necessary before d. c. stability could be achieved by means of the feedback network.

(g) The a. c. Amplifier.

The bandpass of the feedback network does not extend beyond 20c/s, but nevertheless appreciable phase shifts at lower frequencies occur in passing through the generator. To eliminate hunting at high feedback gain, it was necessary to provide some a. c. feedback from the high voltage side of the magnet to the power amplifier.

(vii) Location of the Ring Focus and Baffle Alignment

(a) Location of the Ring Focus

Since there is no exact mathematical treatment of the field form used in the spectrometer, the optimum positions and dimensions of the baffles cannot be calculated. It is therefore necessary to locate the ring focus by the photographic method of ray tracing. To do this, the entrance angle and the source to detector distance were fixed at 30° and 25 cm. respectively. The 30° entrance angle was obtained by using a set of baffles near the source which limited the value of α to

$30^{o} \pm 2^{o}$. The one inch detector was stopped down to 4 mm. by means of a brass plate with a hole in it located axially on the axis, and a lead shield was placed between the source and detector. A 2mm. diameter source of Cs^{137} was then mounted in the source position and the current required to focus the K conversion line of the 661 kev transition was determined. This experiment gives the current necessary to bring an electron of energy 624 kev emitted at 30^{o} to the axis back to the axis again at the position of the detector. Strips of X-ray film were mounted in the vacuum chamber in a plane containing the axis of symmetry and an exposure of several hours was made to register the profile of the electron beam on the film, using this current setting. These photographs showed the ring focus very clearly, the K and L conversion electrons registering in narrow lines of width about one mm. located 2 mm. apart on the film. The beam on both sides of the ring focus became very diffuse but was sufficiently well defined to show that there was adequate clearance between its outer edge and the wall of the vacuum chamber. The clearance was not sufficient to warrant choosing a larger mean angle of emission than 30^{o}. Since the performance is not very sensitive to changes in this angle (34), this limitation is of no importance. A comparison of the experimentally located ring focus position with that expected from theory has already been made in Chapter II.

(b) Baffle Construction and Alignment

The details of construction of the Hubert baffle (see Chapter II) are presented in Figure 15. Its outer jaw is a fixed cone with a slope that matches the profile of the ring focus. Its inner jaw is a disc of 1/4" brass of diameter equal to the width of the ring focus and bevelled to match the outer cone. The inner jaw

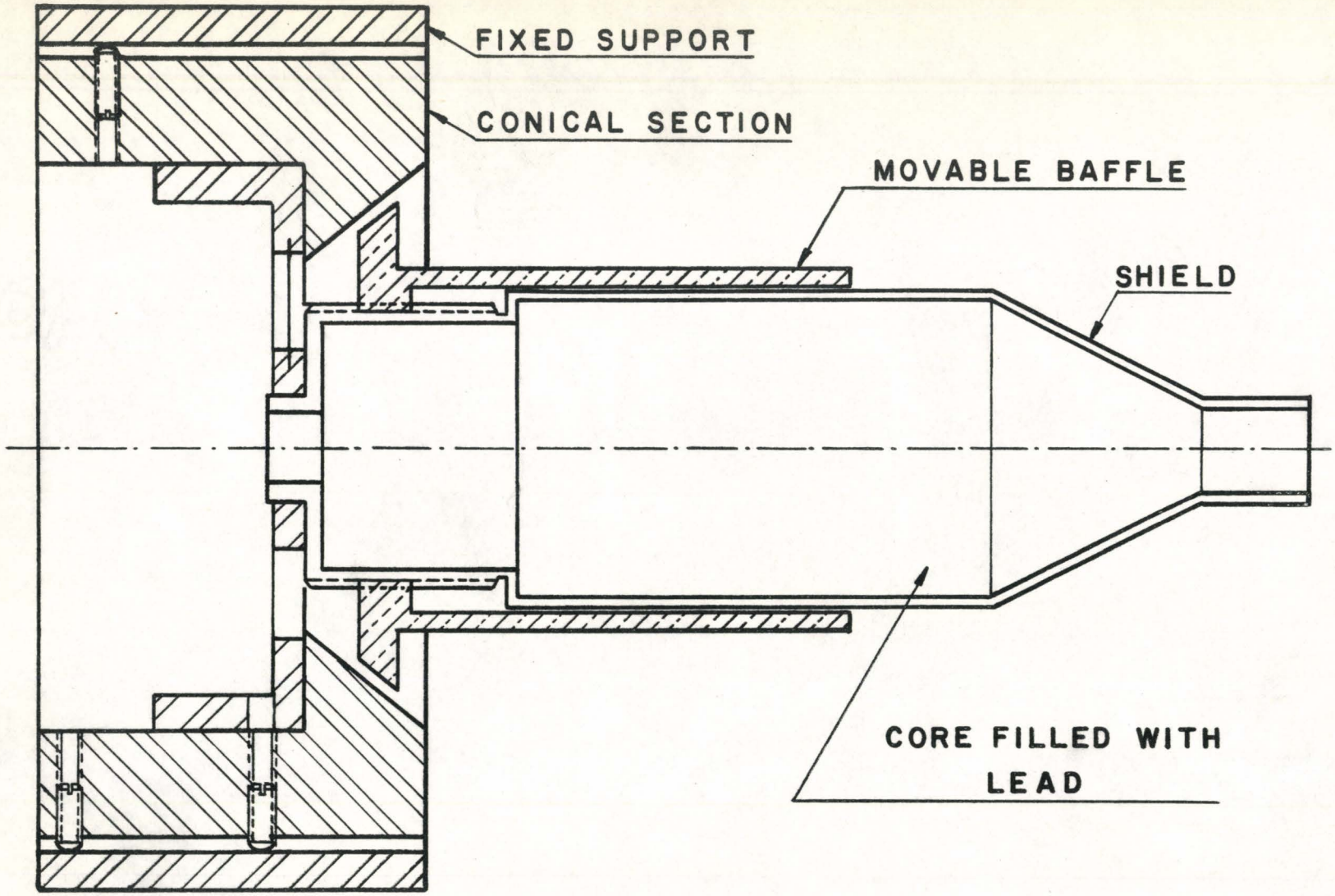

FIG. 15 HUBERT BAFFLE

is mounted concentrically with the outer cone on a threaded shaft so that the gap between the two jaws can be varied continuously and reproducibly simply by rotating the inner jaw. Since the baffle must be accurately located with respect to the electron beam, provision is made for moving the entire baffle system laterally and vertically with respect to the instrumental axis. The baffle system was adjusted to concentricity with the electron beam axis in the following manner. With the baffle in place a brass plate with a 45^{o} sector removed was placed between the baffles and detector to allow only electrons passing through one quadrant of the ring baffle to be recorded. The conversion line was then scanned four times, recording in turn the electrons passing through each of the four quadrants of the ring baffle. The criterion for correct alignment is that all four peaks occur at the same magnet current. A typical case illustrating a poor and a well aligned baffle system is shown in Figure 16. The pairs of curves in the left and centre of this Figure show peaks as recorded in each of the four quadrants with poorly aligned baffles. The shifts between the North-South peak positions correspond to a misalignment of 0.34 mm. After making the appropriate corrections the four peaks fall directly on top of each other as in the curve on the extreme right. The width and height of this curve cannot be directly compared with the other four as the baffles had been stopped down to increase the sensitivity of the test. The position of the peak has also moved slightly demonstrating the fact that with the Hubert baffle the line position depends on the baffle setting.

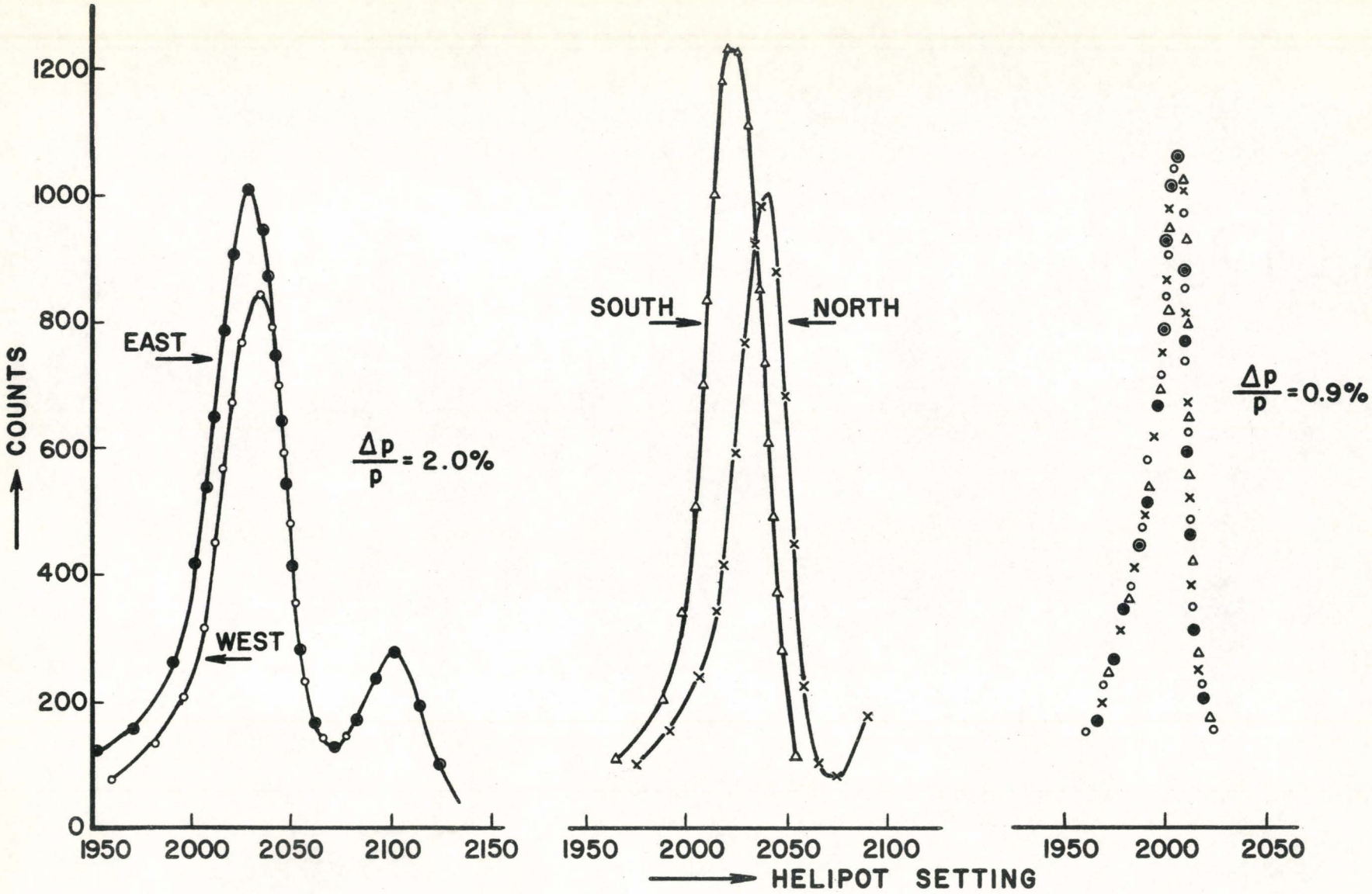
1200
1000
800
600
400
200
0
COUNTS
EAST
WEST
$\frac{\Delta p}{p}$ = 2.0%
SOUTH
NORTH
$\frac{\Delta p}{p}$ = 0.9%
1950
2000
2050
2100
2150
HELIPOT SETTING

FIG. 16

(viii) Determination of the Spectrometer Transmission

(a) Determination of Transmission

When once the field shape, the source position and the detector position and diameter have been chosen, the transmission of the spectrometer for a point source depends only on the size of the ring focus aperture and (or) the diameter of the entrance baffle. In the present instrument, the entrance baffles do not critically define the electron path so that the transmission for a point source is a function of the ring focus aperture alone. With this aperture wide open, the instrument has its maximum transmission, a value which is independent of the source diameter providing it is small compared to the detector diameter (i.e. small compared to 2.5 cm.). With the ring focus aperture partially closed, the transmission does change significantly with source dimensions. It is thus possible to determine the maximum transmission once for all, but it is necessary to determine the actual transmission with a partially closed ring aperture for each source placed in the spectrometer, by observing the counting rate in a conversion peak as a function of the baffle setting.

The maximum transmission was determined by placing a Cs^{137} beta source of known strength in the spectrometer and measuring the counting rate on the K conversion peak of energy 624 kev when the baffles were wide open. The transmission at other baffle settings was similarly measured. It should be emphasized that while the maximum transmission so determined is a property of the spectrometer independent of source size, the transmissions found for partially closed baffles depend strongly on source size.

The results of these determinations are presented graphically in Figure 17

SPECTROMETER No. 1

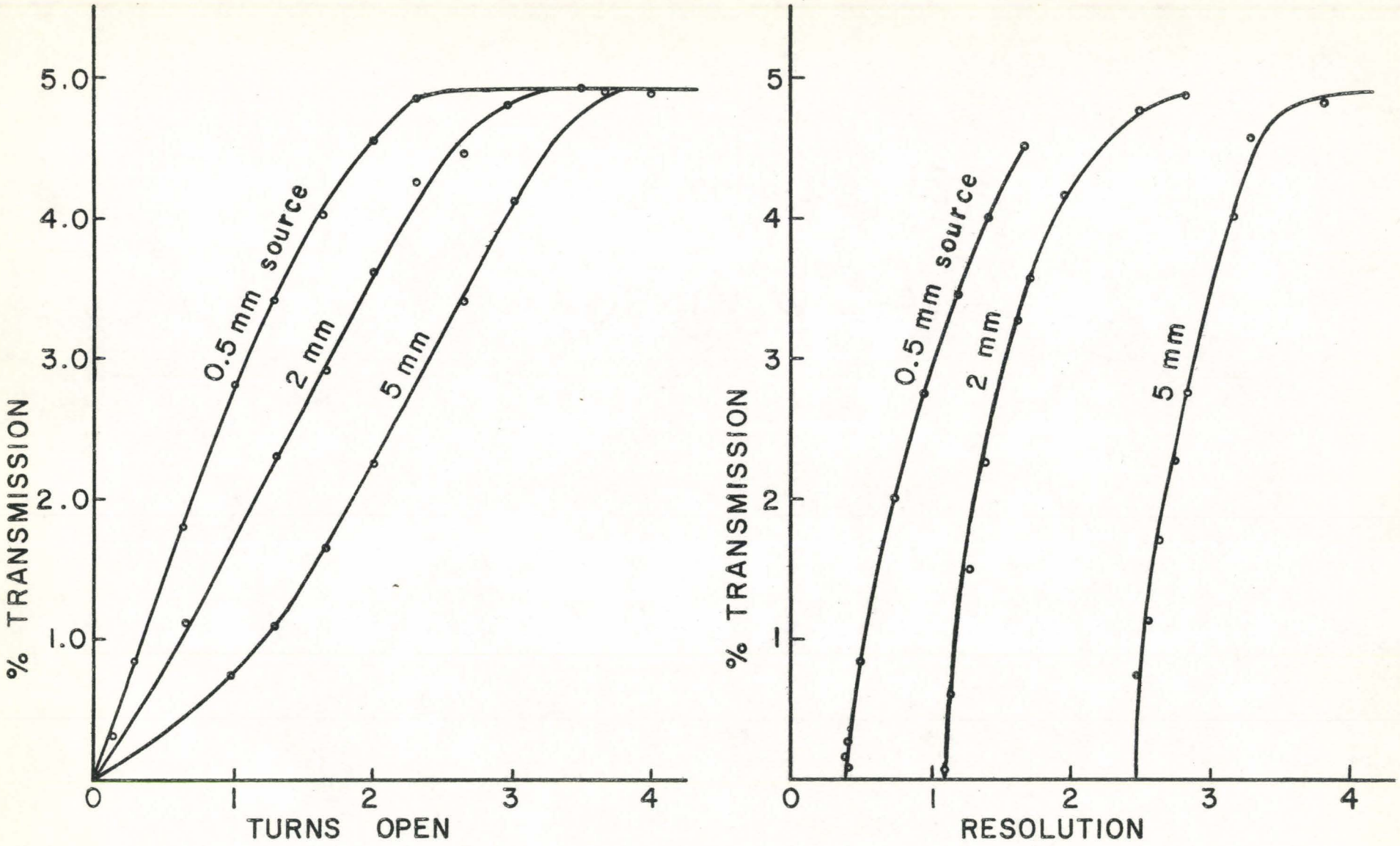

FIG. 17

for one spectrometer only. The results for the other are very similar. The curves for transmission vs "turns open" show clearly that the transmission at a given baffle setting depends on source size but that the maximum transmission is a constant of the instrument limited by the detector diameter. The 5% maximum transmission could conceivably be increased to 7% if one could design a light pipe capable of working with a larger detector.

The resolution-transmission curves show clearly the effect of source size on performance. The 0.4% resolution obtainable with the point source is not really very practicable for coincidence work since the transmission is too low. In practice, one usually works with sources of diameter 2 - 5 mm., which means resolutions and transmissions in the range of 2 to 4%.

(b) Determination of Source Strength

Inasmuch as the determination of the Cs^{137} source strength in the most difficult part of the procedure outlined above, the method used is described in some detail below.

A small source of Cs^{137} of diameter less than 1 mm. was prepared on a Mylar film and mounted on the spectrometer source mounting plate. Two anthracene crystals of dimensions 2.5 x 1.3 x 1.3 cm. were wrapped in aluminum coated mylar (on all but one face) and mounted side by side on a RCA 6810 held in a vertical position. The source was then placed between the two crystals as shown in Figure 18, to give essentially a 4π counting geometry, (a correction of 1.2% was applied for the lack of complete 4π geometry), and the entire assembly enclosed in a light tight box. The pulse height spectrum was then observed

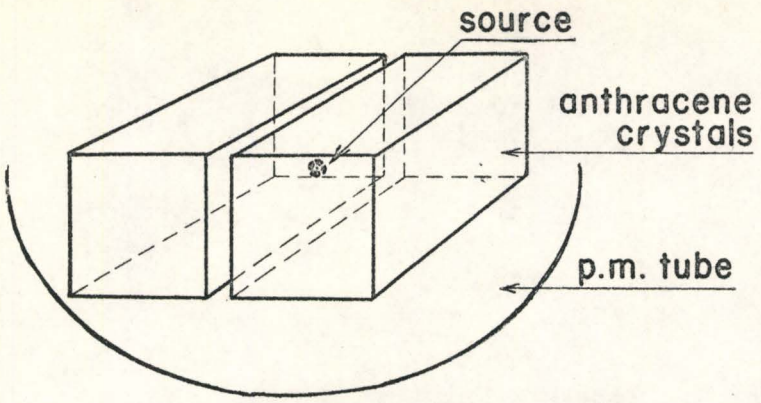

Figure 18

using a single channel pulse height analyser. To correct for the effect of the gamma rays the spectrum was repeated with the source sandwiched between 0.5 gm/cm^2 brass plates. Finally, the integral spectrum above the lower edge of the window was measured in order to make the results independent of the window width calibration of the analyser. One such set of data is presented in Figure 19. Curves A and B represent the total and gamma spectra respectively, (Curve D the integral spectrum) and the difference represents the pulse distribution due to the beta ray and conversion electron spectrum of Cs^{137}.

The decay scheme of Cs^{137} is very well known. The radiations involved are as follows (see Nuclear Data Sheets, N.R.C., Washington) :

(a) a main group, with intensity 92% and energy 0.51 Mev;

(b) a weaker group, with intensity 8% and energy 1.18 Mev;

(c) a 0.661 Mev gamma ray, with the total K+L+M conversion coefficient of 0.108. Of the total conversion electron intensity, 82% is due to K electrons.

Since, in the transmission determination, we are only concerned with the number of K conversion electrons emitted by the source, there is no necessity to use any of the published branching ratios except to make a correction for the

number of high energy beta rays underlying the conversion electron peak and to use the 82% figure given above to obtain the number of K conversion electrons in that peak. From the data above, the high energy beta group has an intensity equal to 74% of the conversion electron intensity. This spectrum spreads from 100 kev to 1.2 Mev in the manner shown by Curve C in Figure 19 (calculated from the Fermi theory) and roughly one-fourth of the total underlies the conversion electron peak. It is estimated that uncertainties in the branching ratio for this beta group and in the method of analysis introduce an uncertainty of 4% in the conversion electron source strength. Inasmuch as three independent determinations of this source strength, all analysed in the same way, gave results agreeing within 4%, it is felt that the conversion electron source strength of the Cs^{137} source is known to within 6%. The averaged result of all determinations is:

$$N = 2105 \pm 120 \text{ K conversion electrons/second}$$

for the source used in calibrating the spectrometer.

(ix) Scattering

It was early recognized that a weak, low energy tail extended beyond the end-point of a simple beta spectrum. The counting rate in this tail was sometimes as large as 1% of the counting rate on the maximum of the continuum and was reduced sharply as the baffles were closed. This tail was entirely removed when the source was covered with an aluminum absorber, showing that it was due to electrons scattered from the walls of the vacuum chamber and not to gamma rays. In determining the end point of a beta spectrum it was necessary to allow for the effect of this "tail" to get the correct end-point and hence its presence reduced the accuracy

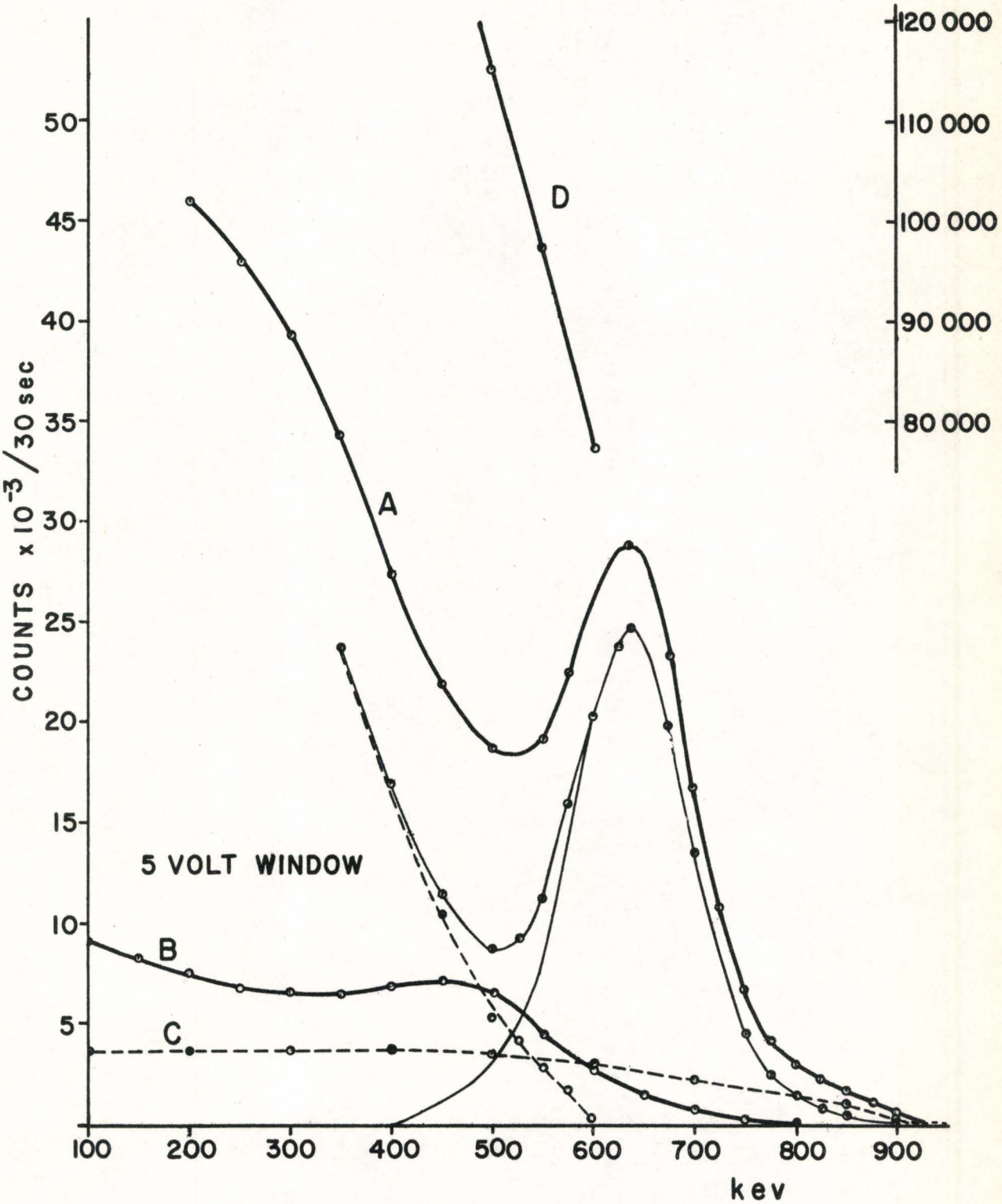
120 000
110 000
100 000
90 000
80 000
50
45
40
35
30
25
20
15
10
5
COUNTS x 10^-3 / 30 sec
A
B
C
D
5 VOLT WINDOW
100
200
300
400
500
600
700
800
900
kev

FIG. 19

with which these end-points could be determined.

It was assumed that this scattering was an inherent defect of a spectrometer of small dimensions. However, after these experiments were completed, a systematic attack on the source of this effect by Dennis Burke of this laboratory led to a complete understanding of its cause and to its removal by a suitable baffle between the ring focus and the source. Since this baffle was added, no measurable trace of the effect remains.

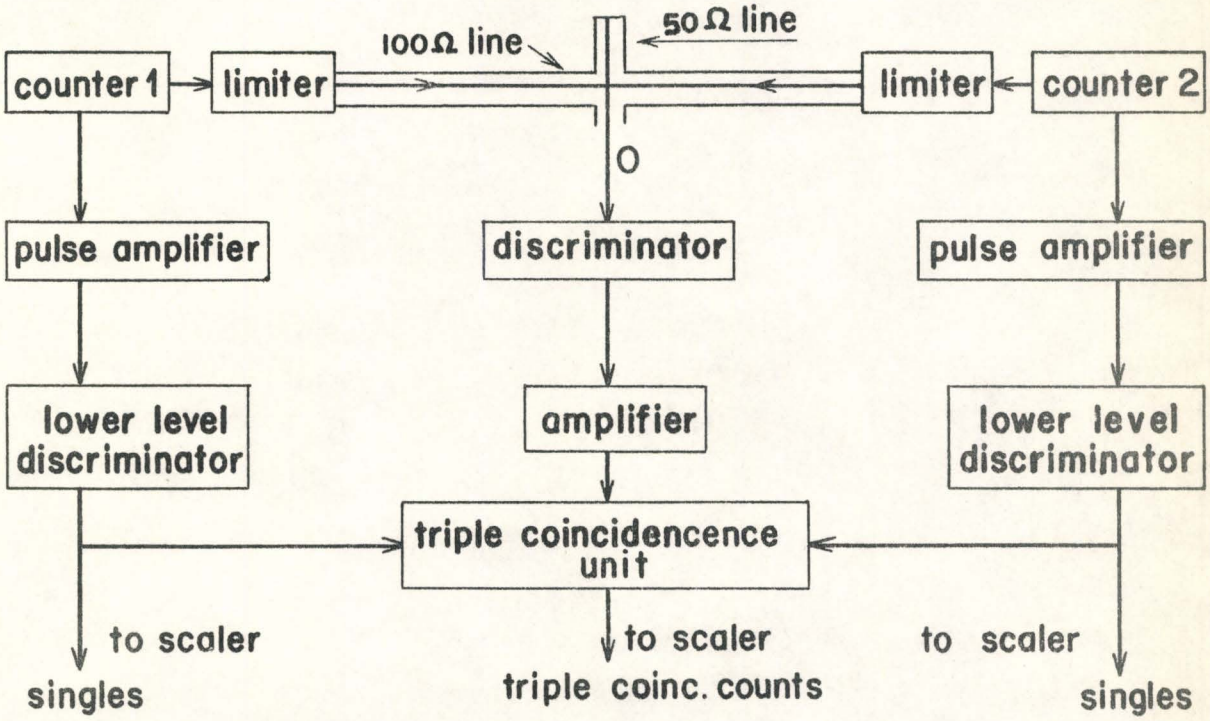

Figure 20

(x) The Coincidence Circuit

The coincidence circuit of the Bell, Graham and Petch, type (35) was set up as shown in the block diagram of Figure 20. The electron detectors were anthracene crystals coupled to RCA 6810 photo multipliers. The gain of this tube, when operated at 2000 volts, is sufficient to ensure that the limiter will be cut off by the pulse due to the first photoelectron to leave its photocathode. (The

total pulse height was $\sim$ 50 volts for 100 kev electrons). The clipped output pulses from the (404A) limiter are positive pulses of uniform height ($\sim$0.75 volt), uniform length ($\sim 10^{-7}$ sec) and very fast rise time ($< 10^{-9}$ sec). Unfortunately, these 6810 tubes turned out to have a very large time jitter (of the order of 5 mμ sec) which made it impossible to make full use of the properties of these pulses.

The pulses from the limiter pass down the 100 ohm line, are reflected by the 50 ohm stubbing cable, and, together with the reflected pulses, create pulses at O of height $\sim$ 0.37 volts and duration 2τ, where τ is the time taken for a pulse to travel down the stubbing cable. The reflected pulses pass to the anode of the limiter and are absorbed in the terminated line.

When pulses from both counters arrive at O simultaneously, a pulse of double the standard height is produced. If the center channel discriminator is adjusted to reject the standard pulses but to pass the double height ones, only coincidence pulses will be passed by the center channel. The resolving time of the fast circuit is determined by the length of the stubbing cable and the level of discrimination in the center channel (i.e. the degree of overlap of the incident pulses demanded by the center channel).

The pulses for the side channels are taken from a dynode near the anode of the photomultiplier, amplified and passed through a lower level discriminator and fed to the triple coincidence circuit and to a scaler. The triple coincidence unit rejects essentially all of the coincidences due to noise in either photomultiplier.

The process of setting up the circuit for an experiment involves three

steps. The first is to set each spectrometer on the position of the spectrum to be investigated and determine a bias curve. Curve (a) of Figure 21 shows a typical bias curve for the L-conversion peak of the 139 kev transition. It is clear from the curve that essentially 100% detection efficiency can be achieved without accepting much noise. For lower energy electrons, the plateau is shorter but quite workable for electrons down to 40 kev.

The adjustment of the coincidence circuit is slightly complicated by the fact that transit time of the electrons through the trajectory of 29 cm. length ranges from 1 mμsec. at high energies to 3 mμsec. at 30 kev. With the 100 ohm cable lengths adjusted to bring pulses from prompt coincidence events into coincidence at O, a center channel bias curve is taken (as in Figure 21 (c)). It is seen from the figure that again there is a good plateau. The shape of this curve is quite insensitive to the energy of the electrons which produce the coincidences, and the bias setting need not be changed throughout an experiment. With an appropriate setting of this bias, a resolution curve such as Figure 21 (b) is obtained by altering the lengths of cable between the photomultipliers and the fast coincidence unit. In order to be certain that the coincidence efficiency is 100%, it is essential that the resolution curve have a flat-topped portion and that the operating point be chosen near the center of this portion. In the experiments described in Chapter V, resolving times of 12 and 16 mμseconds were used.

The chance contribution to the coincidence rate may be measured directly by interposing a long delay in one coincidence channel or may be calculated from the relation $N_c = 2N_1 N_2 \tau$ where N_1 and N_2 are the side channel rates. In

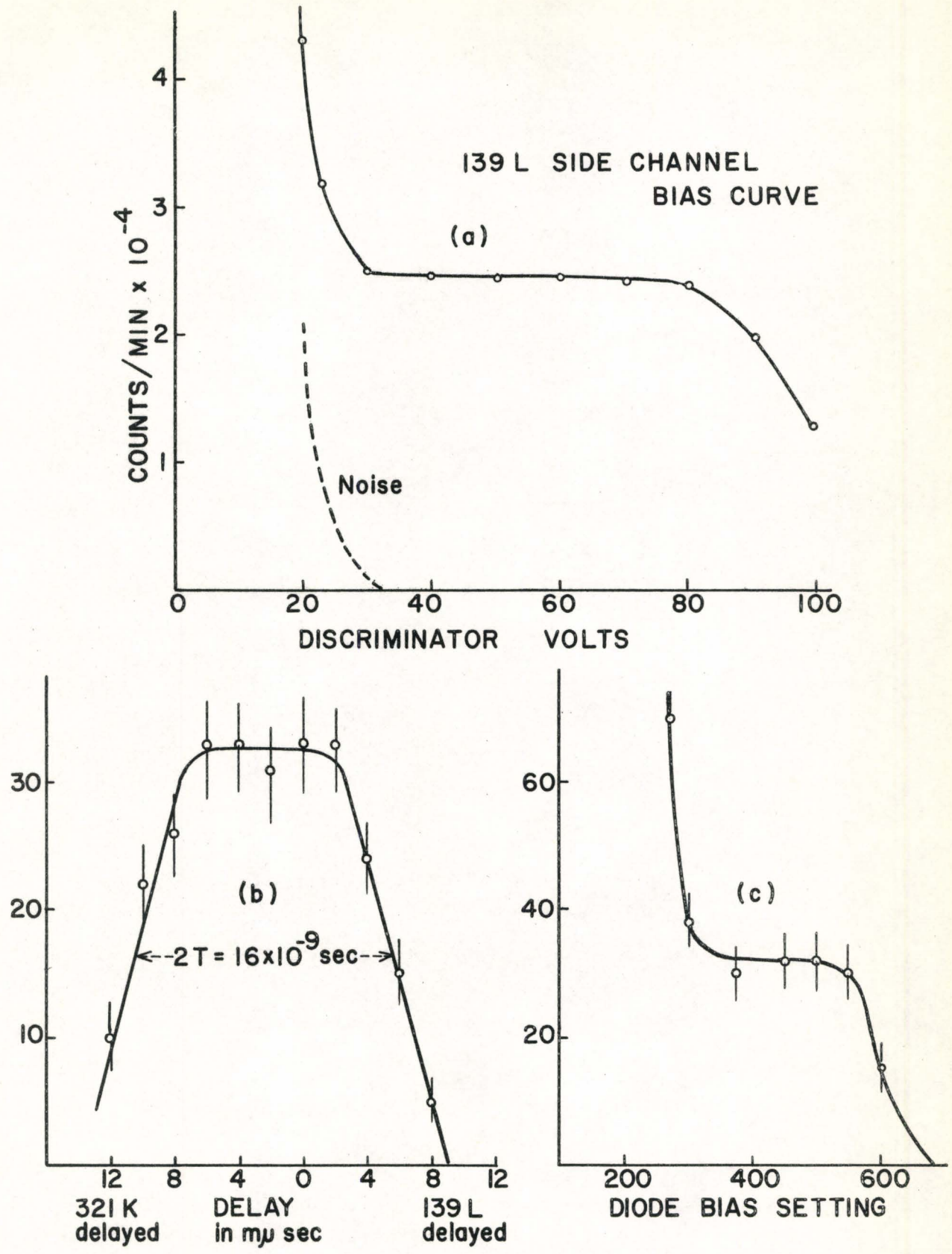
139 L SIDE CHANNEL
BIAS CURVE
(a)
COUNTS/MIN x 10^-4
Noise
DISCRIMINATOR VOLTS
(b)
-2T = 16x10^-9 sec-
321 K delayed
DELAY in mμ sec
139 L delayed
(c)
DIODE BIAS SETTING

FIG. 21

practice, both methods were used, a few measurements of N_C being performed during the experiment to check that the theoretical relation was valid.

While, in principle, one might have reduced the resolving time and so made possible the use of stronger sources there was, in fact, little advantage in doing so, since the specific activities of osmium obtainable were so low that source thickness effectively limited the strength of sources that could be used. On the other hand, a reduction by a factor of 2 might have created a serious loss in efficiency for coincidences with the 73 kev transition with its lifetime of 6.0 ± 0.4 mμ sec (38).

CHAPTER V

THE BETA DECAY OF Os^{193}

(i) Introduction

The decay of Os^{193} has been studied by several workers (36). Relatively complete investigations have been carried out by Cork et al (37), de Waard (38) and Nablo (39). Cork determined the energies of a large number of conversion lines using permanent magnet spectrographs. De Waard carried out coincidence experiments using a long lens spectrometer to focus the conversion lines and an anthracene scintillation spectrometer for the beta continuum. The resolution of the anthracene spectrometer was very poor and the end-points of the spectra were subject to large uncertainties. Nevertheless, on the basis of his coincidence data and the accurate measurements of Cork et al , he proposed levels at 73, 139, 281, 387 and 460 kev. Subsequent work by Nablo, however, revealed the presence of eleven gamma rays not previously detected. All but six of these could be fitted into four of de Waard's levels. Nablo was therefore led to postulate three additional levels at 247, 315 and 613 kev to account for these transitions on the basis of energy fit alone. (See Figure 22 for Nablo's decay scheme). He rejected de Waard's level at 387 kev which could account for the 106, 248, 314 and 387 kev transitions, because it involved using the last named transition twice. None of the energy measurements have been precise

(A)
The Os^{193} internal conversion spectrum above 1500 gauss-cm.

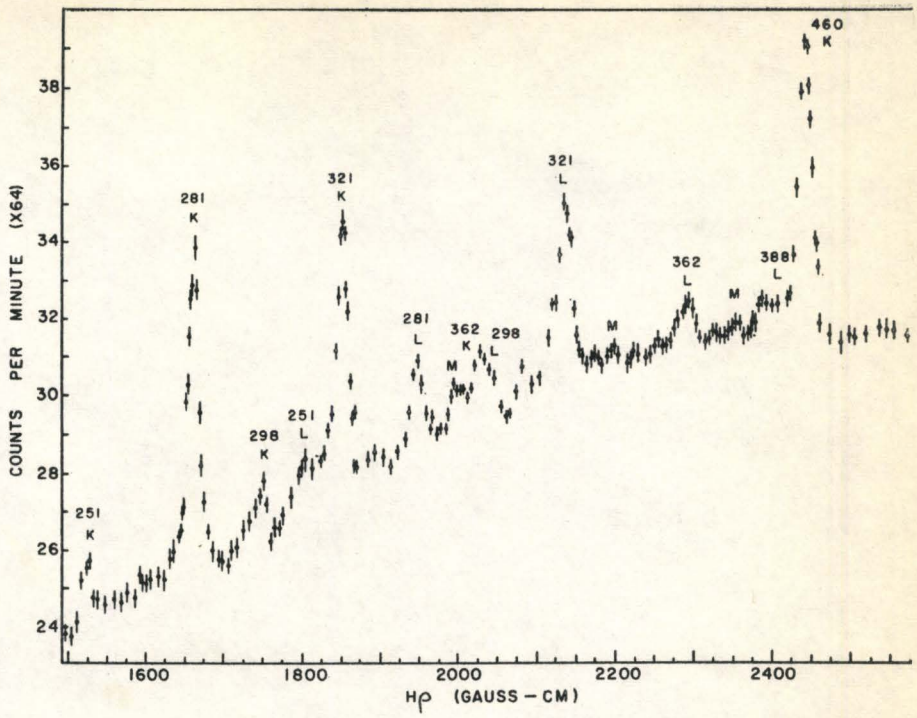

(B)
The low energy internal conversion spectrum of Os^{191} and Os^{193}. The spectrum as recorded about one day after irradiation is dominated by the strong 0.0742-Mev isomeric transition. The insert shows details of two weak conversion peaks between the 0.129 K and L peaks.

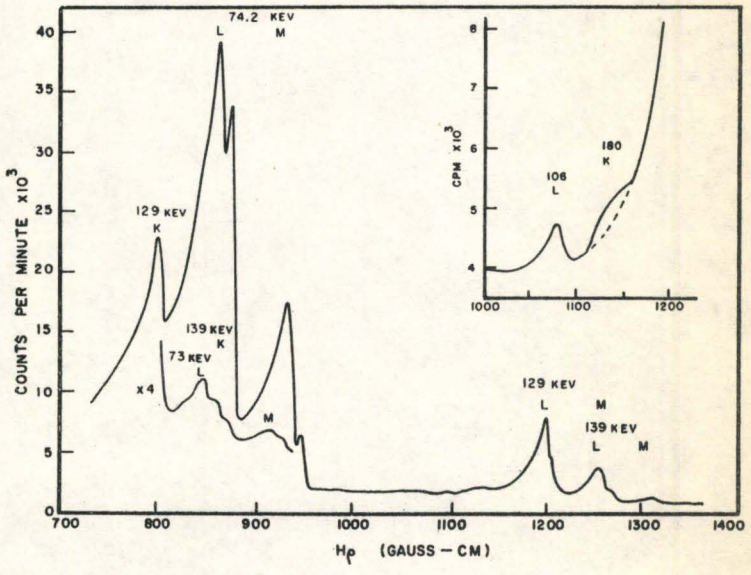

(C)
Beta-gamma coincidence spectra as recorded with the scintillation spectrometer. (A) Beta rays in coincidence with the 0.559-Mev gamma ray.

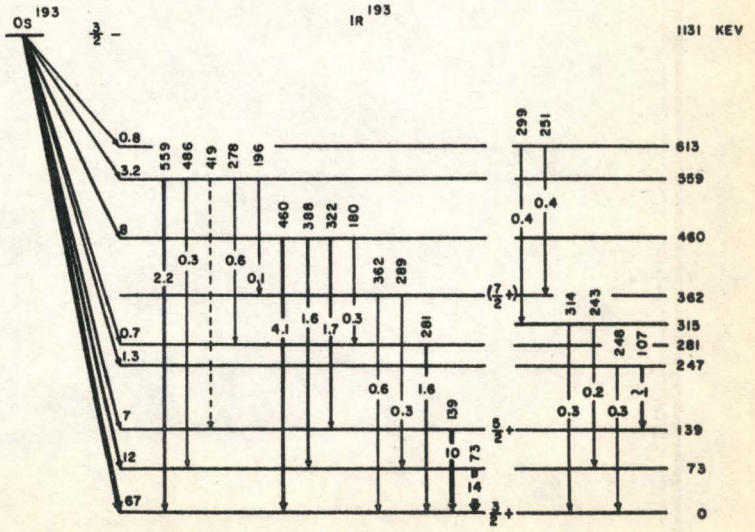

FIG. 22.

enough to force a decision between these two choices. Nablo analysed the beta spectrum into five groups and established the branching ratios to most of the excited states. He also made an independent assessment of these branching ratios through an extensive series of gamma ray measurements. There exists a serious discrepancy between these values and those obtained from beta ray measurements which he could not resolve.

Nablo's experiments ran into two major difficulties: the subjective nature of the Fermi analysis for a complex beta spectrum and the presence of the intense beta spectrum of Os^{191} which extends up to 143 kev. (Separated isotopes of osmium are not yet available). Since the electron-electron coincidence experiments simplify the first problem and eliminate the second, it was felt that these experiments might be able to resolve the inconsistencies in Nablo's decay scheme. Inasmuch as his energy measurements are superior to any that could be obtained with the coincidence spectrometer, the present work has leaned heavily on his energy and conversion electron data. Figure 22 shows the internal conversion spectrum as observed by Nablo at a resolution of 0.6%. The peaks in this spectrum stand up more sharply than in the single spectrum of the coincidence spectrometer and will be useful for reference.

(ii) Source Preparation

Osmium metal, in the form of a powder, was sealed in quartz capsules and irradiated in the Brookhaven reactor for four days at a flux of about 1.8×10^{13} neutrons per cm^2 per second. The capsules were broken under medium-strength nitric acid and the metal dissolved under gentle heating. The solution was then

placed in a beaker and evaporated until fine dark blue crystals of the nitrate began to crystallize out of solution. In the meantime, a thin film of VYNS was deposited on a source holder plate. A drop of insulin was placed on the film, and removed after a few minutes. A drop of the saturated osmium nitrate solution was then deposited on the spot wetted by the insulin and evaporated to dryness. Usually only one drop of solution was used. The size of the source (2 to 5 mm. in diameter) was determined by the size of the initial insulin drop. The same backing in all cases was thin enough that there was no noticeable change in peak position when the source was rotated through 180^{o} (except, perhaps, for the 73 kev L transition).

(iii) Counting Procedure

The coincidence counting rates observed in the following experiments ranged from 1 count/min. to 20 counts/min. while the single channel rates were of the order of a thousand to 100, 000/min. In recording coincidence data, it became standard procedure to count at each point for 15 minutes, and to include a 15-minute chance count about every two hours. Counting was continued day and night with each new source for a period of about five days. The electronic circuits proved to be very stable and it was possible to accumulate data and make decay corrections over the entire period.

(iv) The Determination of the Spectrometer Transmission

Every time a new source was placed in the spectrometer or the baffle setting altered, the transmission was determined in the following manner. The

281 K conversion line was scanned twice, once at maximum transmission and again at the baffle setting to be used in the experiment. For example, in a typical experiment, Figure 23 shows the 281 K peak at maximum transmission and again at a baffle setting of two turns open. From the ratio of the two peak heights the transmission may be directly determined.

(v) The 139 L-β Coincidence Spectrum

Spectrometer No. 1 was set on the 139 L peak and the beta continuum was scanned with spectrometer No. 2. Figure 25 shows the Fermi plot of four such runs normalized to the same counting rate and the analysis of the spectrum into three beta groups with end points of 1000 ± 10 kev, 675 ± 20 kev and 490 ± 30 kev and relative intensities of 1.00, 0.30 ± 0.05 and $.14 \pm 0.05$. If the 1131 kev transition is to the ground state, then these beta groups lead to the states at 139 and 460 kev and to one or both of those at 559 and 613 kev. (See Figure 22). Moreover, one would expect to find the 322 kev transition between the 460 and 139 kev levels. This expectation was confirmed by observing direct coincidences between the 322 K and 139L conversion electrons (Section (v) (b)). The strength of the 490 kev beta group suggests that the transitions from the upper levels (559 and (or) 613 kev levels) are stronger than is indicated by Nablo's decay scheme.

(a) The Conversion Probability of the 139-L Electrons

The L-shell conversion probability of the 139 kev transition was determined from the genuine (139L - 322K) coincidence rate and the 322K peak height in the following manner. In Figure 24 let λ_1 and λ_2 refer to the 139 L and 322 K conversion peaks and let 1a, 1b and 2a, 2b refer to on-peak and off-peak momentum

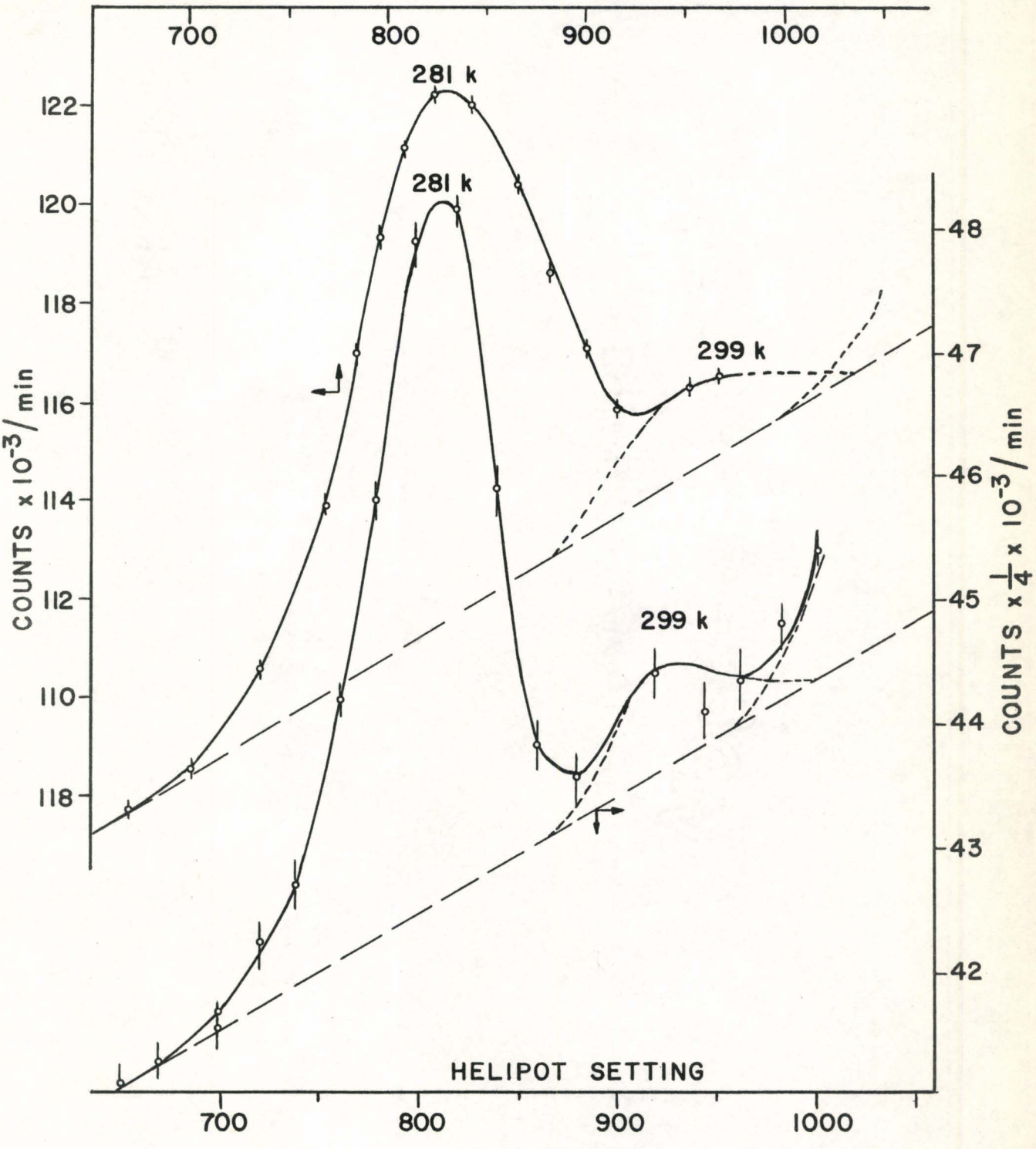
700
800
900
1000
281 k
281 k
299 k
299 k
122
120
118
116
114
112
110
118
48
47
46
45
44
43
42
COUNTS x 10⁻³/min
COUNTS x ¼ x 10⁻³/min
HELIPOT SETTING
700
800
900
1000

FIG. 23

321 K – 139 L COINCIDENCE

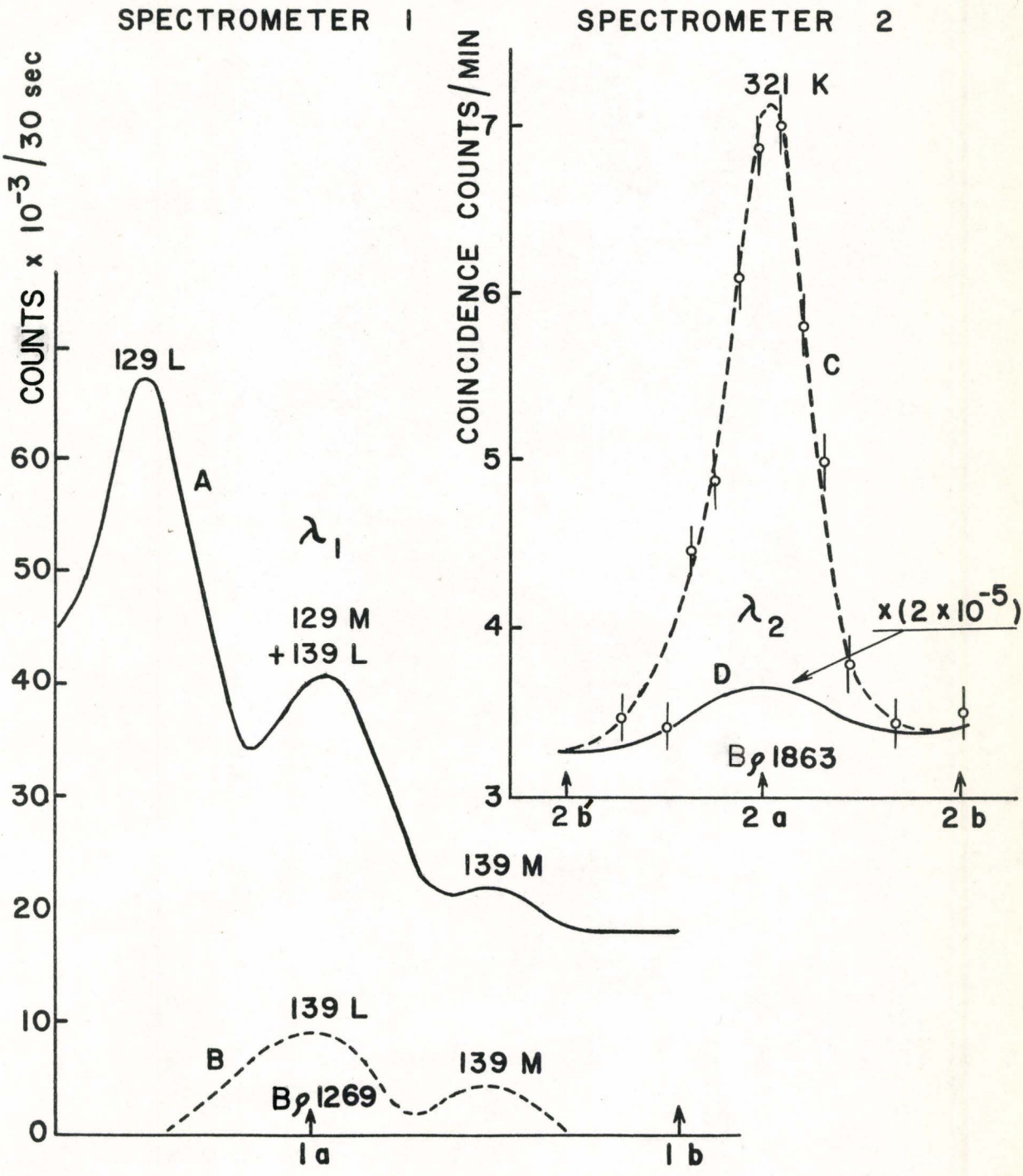

FIG. 24

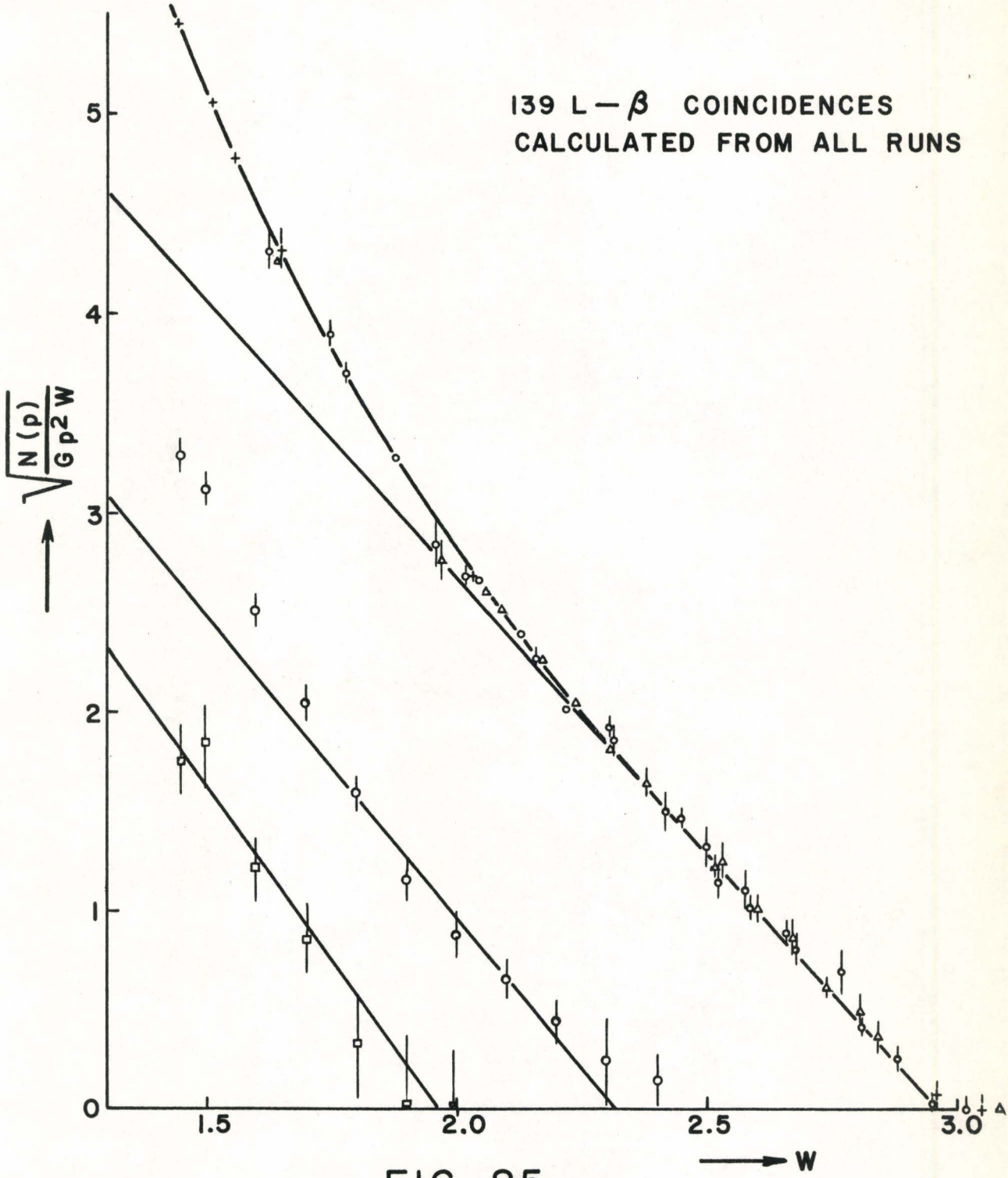
139 L — β COINCIDENCES
CALCULATED FROM ALL RUNS
$\sqrt{\frac{N(p)}{G p^2 W}}$
0
1
2
3
4
5
1.5
2.0
2.5
3.0
W

FIG. 25

settings for λ_1 and λ_2 respectively. It was shown in Chapter III that:

$$\omega_1 \kappa_{139L} = \frac{N(\lambda_1 \lambda_2)}{N(\lambda_2)}$$

However, this result is only true if the line is not broadened by source thickness. In the case of the 139-L peak, there was significant broadening and so the expression above becomes:

$$f\omega_1 \kappa_{139L} = \frac{N(\lambda_1 \lambda_2)}{N(\lambda_2)}$$

The quantity f was evaluated by measuring the area of the composite 129L + 129M + 139L profile, and deducing the peak height which would give the same area if source broadening had been absent.

While in Curve C, Figure 24, the complete coincidence peak profile is established, this is not necessary since all we need are the peak heights. It is more economical of counting time to measure only the rates at points such as 1a, 1b and 2a, 2b and 2b′ of the figure.

The Table below records the various measurements used in determining κ_{139L}.

Table 1

f	=	0.51
ω_1	=	1.86 %
$N(\lambda_1)$	=	5048 c/m
(1a - 2a)	=	$N(\lambda_1\lambda_2 + \lambda_1\beta + \lambda_2\beta + S^*)$ = 22.8 ± 0.4 c/m
(1a-2b and 1a-2b^1)	=	$N(\lambda_1\beta + S)$ = 15.0 ± 0.2 c/m
(1b - 2a)	=	$N(\lambda_2\beta + S)$ = 4.5 ± 0.3 c/m
(1b-2b and 1b-2b^1)	=	$N(S)$ = 1.1 ± 0.3 c/m
whence $(\lambda_1\lambda_2)$	=	4.3 ± 0.6 counts/min.

*The scattering rate.

The value of κ_{139L} deduced from this data is 8.6 ± 0.6 %.

(d) The Branching Ratio for Betas Feeding the 139 kev Level

If spectrometer #1 is focussed on the 139 L line, and spectrometer #2 on the beta continuum, we saw in Chapter III that:

$$\frac{(139L - \beta)\text{area}}{(\beta)\text{ area}} = \delta_{139}\, \varkappa_{139L}\, f\omega_1$$

However, if the 139L – 322K coincidence experiment is done with the same source and under the same conditions as the 139L-β coincidence experiment, δ_{139} can be determined directly without evaluating either $\varkappa$ or $f\omega$ separately.

Moreover, since the shape of the spectrum in coincidence with the 139L transition is very well known and independent of source size and resolution to within rather wide limits (see Figure 25), then the coincidence counting rate at any point is sufficient to give the area under the coincidence continuum. Similarly, the singles channel counting rate at a given point is sufficient to give the area of the single channel continuum.

Thus one can show that:

$$\delta_{139} = \frac{(\lambda_1 \beta)\text{ area}}{(\beta)\text{ area}} \times \frac{N(\lambda_2)}{N(\lambda_1 \lambda_2)}$$

$$= \frac{R_c}{R_s} \cdot \left[\frac{N(\lambda_1 \beta)}{N(\lambda_1 \lambda_2)} \right] \Big/ \frac{N(\beta)}{N(\lambda_2)}$$

where R_c and R_s are factors relating the areas of the entire beta spectrum to the counting rates at the points used.

These ratios have been determined for the point 2a of Figure 24. At this point the quantities inside the square brackets are simply the ratios of peak heights to continuum in the coincidence and singles spectrum. The results obtained from three sources are presented in Table 2.

Table 2

Source #	R_c/R_s	$\frac{N(\lambda_1\beta)}{N(\lambda_1\lambda_2)}$	$\frac{N(\beta)}{N(\lambda_2)}$	Weights	δ
1	0.50	1.00	6.7	1	7.5 ± 1.7 %
4	0.50	3.70	19.4	2	9.5 ± 2.0 %
10	0.50	1.98	11.6	2	8.5 ± 1.7 %

Weighted Mean $\delta = 8.7 \pm 0.8\%$

(The weights were determined from the general reliability of the entire experiment since the statistical errors were roughly equal.)

It should be stressed that the 8.7% value of δ_{139} is independent of ω, f, or instrumental resolution. As we shall see, it provides a basis from which a considerable amount of information can be obtained.

(e) The Intensity of the 322 kev Transition.

Once δ_{139} is known the absolute intensity of the inner beta groups of the 139L - β spectrum can be obtained. These values are:

End-Points	Absolute Intensities
1000 kev	$8.7 \pm 0.8\%$
675 kev	$2.6 \pm 0.4\%$
490 kev	$1.2 \pm 0.4\%$

It should be noted that the intensity of the 675 kev group is the intensity of the 322 kev transition since the intensity of cascading transitions from the 460 to the 139 kev level is negligible. This gives us an independent method of assessing Nablo's intensities.

(vi) Transitions to the 73 kev Level

(a) Introduction

The 73 kev transition is masked by the intense conversion line spectrum of Os^{191}. The situation is shown clearly in Figure 22, curve (b). Fortunately none of the masking peaks are coincidence makers and so the possibility exists of obtaining the clean profile of the 73 kev L and the 139 kev K lines in the coincidence spectrum.

Since the specific activity of the Os^{193} sources is low and a thin source is required to avoid source broadening effects it was necessary to work with weak sources and consequently very low coincidence rates. Since with such sources the chance rate was negligible it was possible to begin counting without waiting for the 14 hour Os^{191} isomer to decay.

(b) Profile of the 73L and 139K Conversion Peak

With spectrometer #2 set on the continuum in a region of high counting rate, the coincidence spectrum in the 73L-139K region was scanned with spectrometer #1. Figure 26, (Curve B or C) presents the coincidence data between 800 and 900 $B\rho$. The unresolved 73L and 139 K peaks appear on essentially zero background but show the effects of source thickness. The profile of each of the four lines in this peak can be determined by scanning the 129K peak profile from the same source after the Os^{193} has died away. Figure 26 (Curve A) shows the shape of the 129K peak in a representation of percentage peak height plotted against percentage of peak momentum. Since the positions of the four unresolved peaks are known, one can use Curve A to obtain the fraction of each of the four peak heights contributing at each momentum setting. In addition, for any given

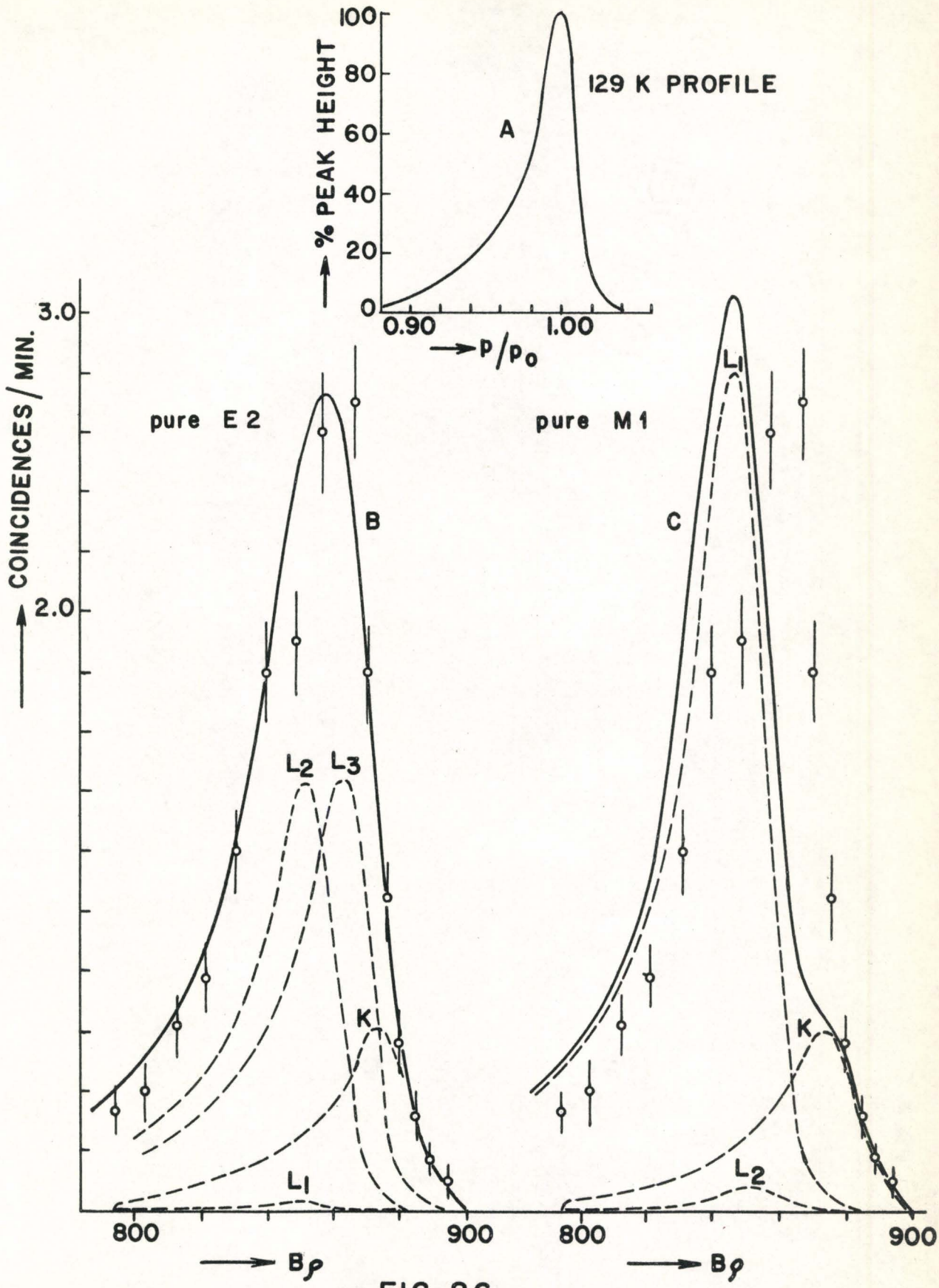
100
80
60
40
20
0
% PEAK HEIGHT
A
129 K PROFILE
0.90
1.00
p/p0
3.0
2.0
COINCIDENCES/MIN.
pure E 2
pure M 1
B
C
L1
L2
L3
K
800
900
Bρ

FIG. 26

M1 + E2 mixture, the $L_1 : L_2 : L_3$ ratios are known. Thus we essentially have a system of three unknowns, namely the peak heights of the 139K and 73L conversion electrons and the mixing ratio, and fourteen equations, corresponding to the fourteen momentum positions chosen. These equations were solved for various values of the mixing ratio. The results showed that no solution is possible if the M1 component in the mixture is greater than 50%. The best fit is given by pure E2.

This conclusion is in agreement with the E2 assignment for the character of this radiation determined by de Waard from a lifetime (38) measurement. In Figure 26, Curve B shows the analysis of the peak for pure E2 and Curve C the best fit possible for pure M1.

The 139K peak height is a small fraction of the total for any mixing ratio and is quite insensitive to that ratio. For pure E2 the 139K peak represents $15 \pm 3\%$ of the total coincidence peak. Since the 139K peak is so small, errors in its value have negligible effect on the interpretation of the 73L coincidence data. Since we know the shape of the 139L-β coincidence spectrum (see Figure 25) and the counting rate associated with 139K-β coincidences at one beta momentum, it is a simple matter to compute the 139K contribution to the total (73L + 139K)-coincidence spectrum for any momentum value.

(c) 73L-β Coincidence Spectrum

To examine the 73L-β coincidence spectrum, spectrometer #1 was set at Bρ860 and the other spectrometer scanned over the beta spectrum. The results obtained after subtraction of the 139K-β contribution are presented in Figure 27. This shows two components with end-points 1040 ± 10 and 675 ± 30 kev

with relative intensities 1.00 and 0.7 $\pm$ 0.1 respectively. The end-points of these two spectra show that they feed levels at 73 and 460 kev, as would be expected from Nablo's decay scheme (Figure 22). The statistical accuracy of the data is insufficient to decide whether or not there are beta rays feeding Nablo's levels at 362 and 559 kev.

(d) The Beta Branching Ratio to the 73 kev Level.

If we accept the pure E2 character of the 73 kev transition as indicated by the strength of the L_3 transition, we can use Rose's tables (8) to obtain the value 0.684 for the total L conversion probability. We can then write:

$$\delta_{73} = \left[\frac{(73L\beta)\text{area}}{(\beta)\text{area}}\right] \Big/ (\mathcal{K}_{73L}\, f\, \omega_1)$$

$$= 3.3 \times 10^{-4} \,/\, 0.684 \times 0.30 \times 0.025$$

$$= 6.4 \pm 1.2\,\%.$$

In this expression f is a factor expressing the percentage of the L's which contribute to the counting rate with the spectrum set at $B\rho$ 860. It is difficult to estimate errors but an uncertainty of 20% seems reasonable.

(e) The Intensity of the 388 kev Transition.

The intensity of the inner beta group of Figure 27 is identified tentatively with the 388 kev transition from the 460 kev level. (Direct coincidences have been observed between the 388K and the 73L conversion electrons but this experiment is not described in detail because it yielded no quantitative measurement.) In the final decay scheme, Figure 33, the 485 kev transition is placed between the 559 and 73 kev levels, so that the intensity of this beta group should include both the 388 and the 485 kev transitions. Using the value of δ_{73} and the relative intensity

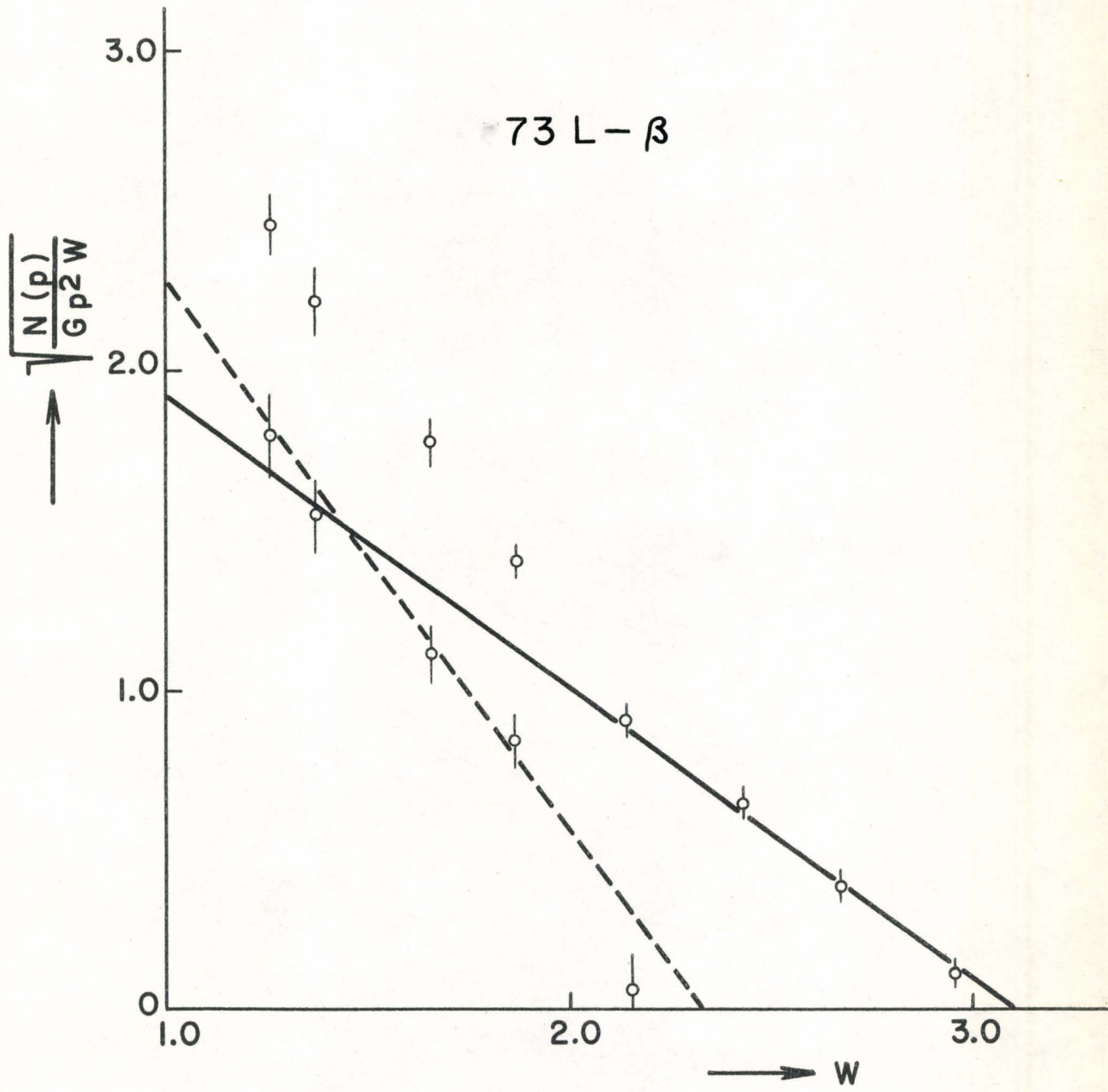

FIG. 27

of this group one obtains directly

$$(\delta_{388} + \delta_{485}) = 4.3 \pm 1.4\%$$

(vii) Transitions from the 460 kev Level.

(a) Introduction.

The experiments on the 139L and 73L conversion electrons described so far have shown that there are beta groups leading directly to levels at 73 kev, 139 kev, 460 kev and from higher levels, 613 and/or 559 kev above the ground state. Also, the position of the 322 kev transition was confirmed by direct coincidences between the 322K and 139L conversion electrons. The position of the 388 kev transition was similarly confirmed. It is also to be expected that the 460 kev transition should go to the ground state, and this is confirmed in the following experiment.

(b) 460K-β and 322K-β Coincidence.

The 460K-β and the 322K-β coincidence spectra were determined by setting Spectrometer #1 on the conversion line in each case and scanning the beta continuum with Spectrometer #2. The Fermi plots obtained are shown in Figure 28. Both spectra appear to be simple with a common end-point at 675 kev in good agreement with the value of 671 kev expected from Nablo's decay scheme. Below 300 kev, it is very difficult to find points in the beta spectrum free of conversion lines. The high points at $W = 1.22$ and $1.37\ Mc^2$ probably include some contribution from conversion electrons and from source thickness effects. There is no real evidence for a low energy component in either spectrum from the data of Figure 28.

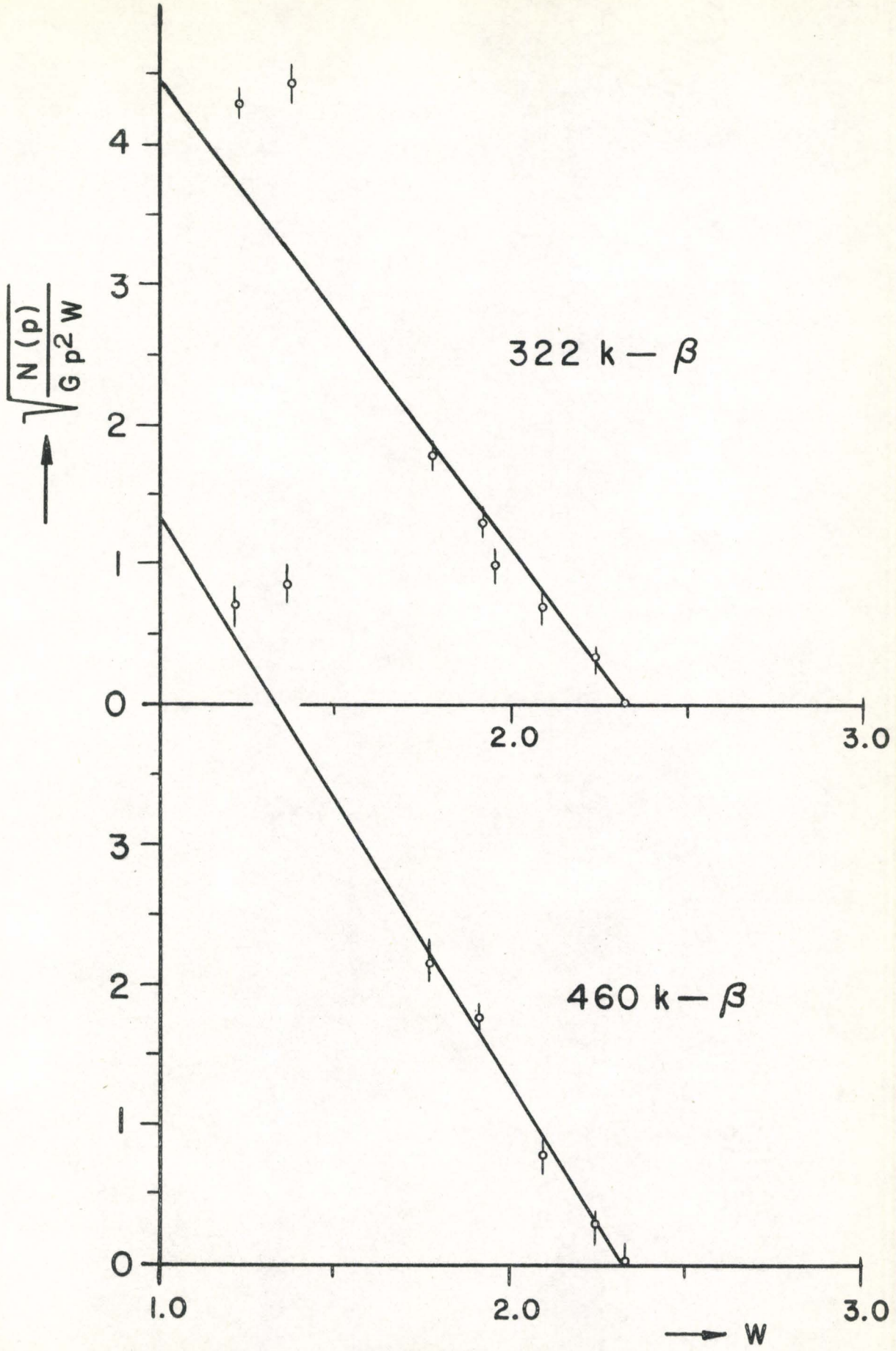

FIG. 28

Using the known solid angle, the areas of the coincidence and total beta spectra, the data leads directly to:

$$\delta_{322}\, K_{322K} = 20 \times 10^{-4}$$

$$\delta_{422}\, K_{422K} = 23 \times 10^{-4}$$

In the case of the 322 kev transition, we can use this result together with the value of δ_{322} obtained in section (v) (e) to obtain:

$$K_{322K} = 0.076$$

This leads directly to a value of:

$$\alpha_K\,(322) = 0.084 \pm 0.02$$

(viii) The (281K + 277K) - Beta Coincidence Spectrum

The 281 K and 277K conversion lines form an unresolved doublet (39). The coincident beta spectrum with this doublet was determined and the results are presented in Figure 29. The spectrum shows two beta groups with end-points of 848 and 548 kev and relative intensities 1.00 and 3.03 respectively, which correspond to the beta's feeding levels at 281 and 559 in Nablo's decay scheme. There is no evidence for a beta group with end-point at $W = 2.32 m_0c^2$, which might be expected as the result of the 180 kev transition in Nablo's decay scheme. This, together with other evidence to be presented later suggests that this line is incorrectly assigned.

The data of Figure 29 suggests strongly that the 277 and 281 kev transitions are in coincidence. The situation is illustrated in Figure 30. In terms of this figure and the areas of Figure 29, $\delta_1 K \lambda_{12} = 6.31 \times 10^{-4}$ (1)

$$\delta_2 K \lambda_2 + \delta_2 K \lambda_{12} = 1.90 \times 10^{-4} \quad (2)$$

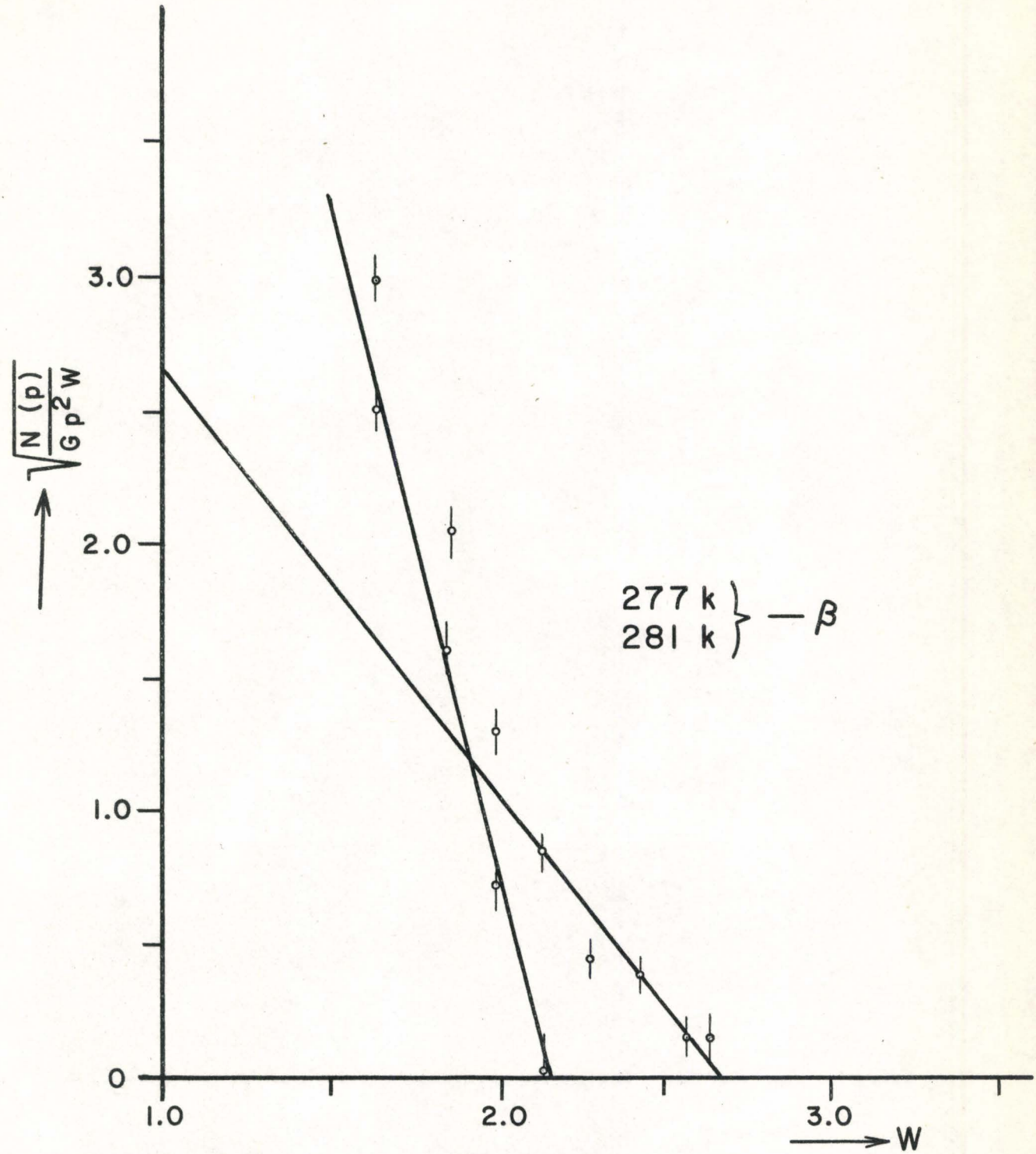

FIG. 29

and therefore

$$(1) + (2), \quad (\delta_1 + \delta_2)K\lambda_{12} + \delta_2 K \lambda_2 = 25.3 \times 10^{-4}$$

This expression is simply the total intensity of the conversion electron doublet and agrees well with the value 28 x 10^{-4} given by Nablo.

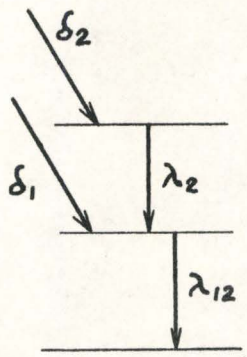

Figure 30

(ix) The 107 and 180 kev Transitions

(a) Introduction

The level at 247 kev was suggested by Nablo (39) to account for the 107kev and 248 kev transitions, but there was no supporting evidence for this level either from the Fermi analyses of the beta spectra or from previously performed coincidence experiments. The 180 kev transition was placed by Nablo between the 460 kev and the 281 kev levels, but the 281K-β coincidence experiment shows that this may not be so. Therefore coincidence experiments were performed with both the 107L and the 180K radiations to determine their positions in the decay scheme.

(b) The 107L-β and 180K-β Coincidence Experiments.

Both the 107L and 180K conversion peaks appear on the low energy side

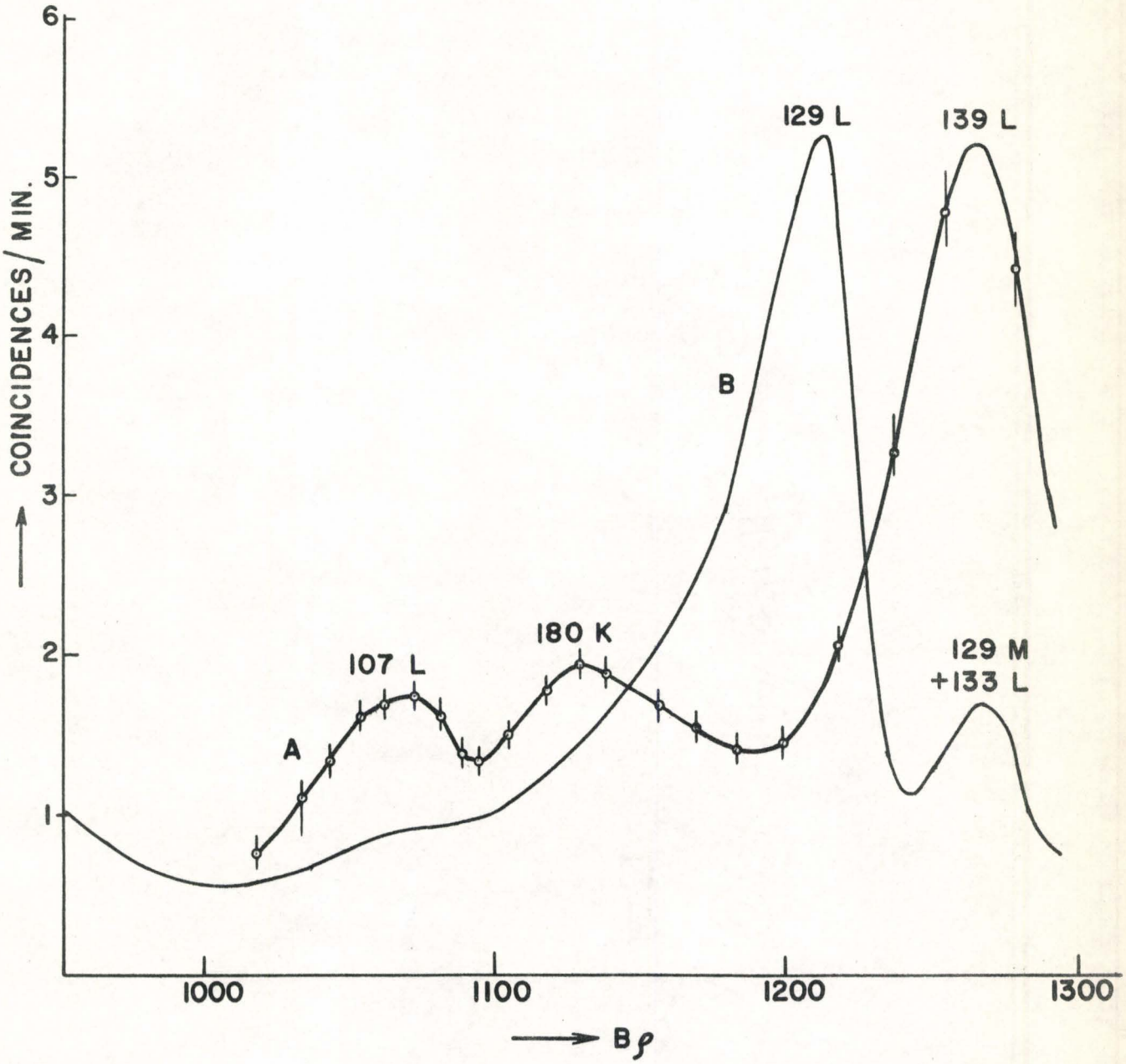
6
5
4
3
2
1
COINCIDENCES / MIN.
129 L
139 L
B
180 K
107 L
A
129 M
+133 L
1000
1100
1200
1300
Bρ

FIG. 31

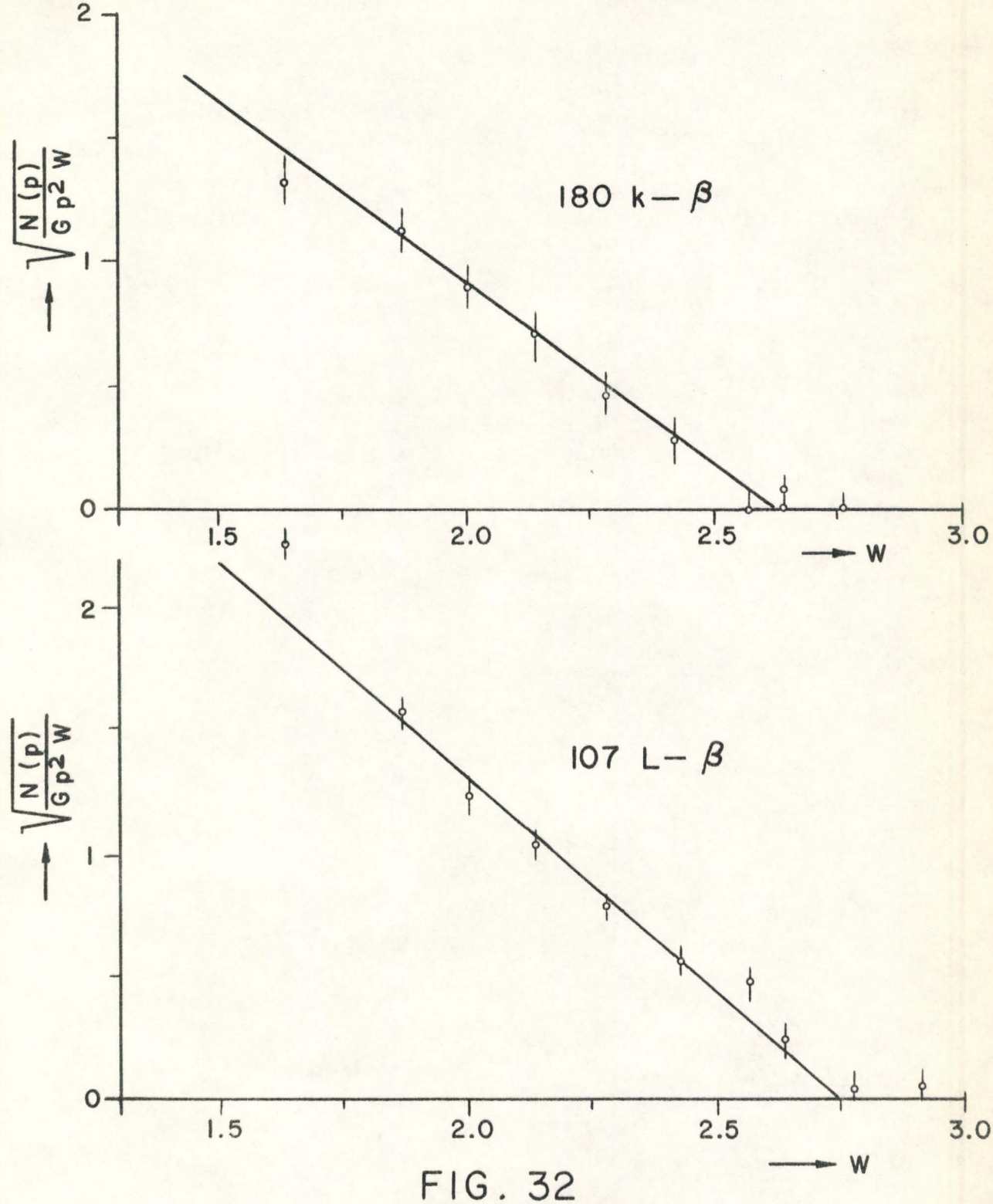

FIG. 32

of the strong 129L line and are difficult to see in the singles spectrum (Curve B of Figure 31). In contrast they show up well in the beta coincidence spectrum as is shown in curve A of Figure 31. The latter curve was obtained by keeping one spectrometer fixed on the continuum while the other scanned the region shown. After the positions of the peaks were so discovered, #1 Spectrometer was set on each peak in turn and the continuum was scanned by Spectrometer #2. Figure 32 presents Fermi plots of the 107L-β and 180K-β coincidence spectra. These are straight lines with end-points at 878 and 827 kev respectively. The end-point of 878 kev indicates a beta group to the 247 kev level and the 107 kev transition proceeds from this level to the 139 kev level. This agrees well with Nablo's suggestion from an energy fit. The data shows however that the 180 kev line is not associated with a beta transition to the 460 kev level, as required by Nablo et al (39), but rather to one at 314 kev. This latter level was originally suggested by Nablo to account for the weak 243, 314 and 299 kev transitions, but finds confirmation in this unexpected manner.

From the coincidence and singles area the values of $\delta_{107}\ \mathcal{K}_{107L}$ and $\delta_{180}\ \mathcal{K}_{180K}$ were found to be $(15 \pm 3) \times 10^{-4}$ and $(18 \pm 4) \times 10^{-4}$ in good agreement with Nablo's values of 21 and 19×10^{-4}. It should be noted that the point at $W = 1.63\, m_0c^2$ falls on the curve for the 180K-β spectrum but considerably higher for the 107L-β. While one hesitates to draw conclusions from one point, this would seem to suggest that there are transitions from higher levels to the 247 kev level but not of comparable intensity to the 315 kev state. This is in direct contradiction to Nablo's decay scheme.

(c) The 107L - 139L and 180K - 139L Coincidence Experiments

If the conclusions in section (b) concerning the positions of the 107 and 180 kev transitions are correct, then both these radiations should be in coincidence with the 139 kev transition. Coincidences were recorded between the 107L and 139L and the 180K and 139L conversion electrons. The low intensity of the 107L and 180K lines as well as the poor signal to noise ratio made these experiments rather difficult. The results obtained are as follows:

	ON the 139L	OFF the 139L	True Peak Ht.
107L	6.8 ± 1.3	2.5 ± 0.9	4.3 ± 1.5
180K	7.2 ± 1.4	4.5 ± 1	2.7 ± 1.7

and show that both the 107 and 180 kev transitions are in coincidence with the 139 kev transition.

This new assignment for the 180 kev transition would indicate that the quoted value of 180 ± 1 kev for its energy is not correct. This is not surprising when one examines the Curve C of Figure 31. The peak shown in the coincidence spectrum of Figure 31 seems to belong to a radiation of 177 ± 2 kev. This value will fit the new assignment quite satisfactorily.

(x) Summary of Measurements

Table 3 presents a summary of the quantities that have been measured in the experiments described. In this table, the nomenclature δ_β (73) refers to the beta transition to the 73 kev level, while δ_γ(388) refers to the 388 kev gamma transition. The second and third columns compare the results for δK obtained in these experiments with those measured by Nablo and Artna (Nablo et al (39)) by a completely different method. Their method involved comparing the area of the conversion peak with that of the total beta spectrum while the present experiments involved a comparison of the area of the coincidence beta spectrum with that of the total spectrum to obtain $\delta K\omega$. The very satisfactory agreement between the two sets of data indicates the correctness of the solid angle determination, and allows one to proceed with confidence to calculations of the δ's. The values of δ_{139} and δ_{322} were obtained by Fermi analysis of the coincidence spectra but are independent of ω or any other geometric factors. The value of K 139L was obtained from a separate experiment and involved the determination of ω. The values of δK for the transitions to the 139 kev level are derived from the measured values of δ and K. The value of δ_{73} and hence $(\delta_{388} + \delta_{458})$ were obtained in a similar way to δ_{139} but involved the spectrometer transmission and the E2 assignment of the 73 kev transition. This assignment was made on the basis of the line shape which fitted a pure E2 but allowed as much as 30% M1 admixture. The value of K_{73L} for pure E2 is 0.68, for a 30% M1 mixture is 0.67 and for pure M1 is 0.51. Thus we see that the value of K_{73L} is very insensitive to the mixing ratio. The other ℓ-β coincidence

TABLE 3

Summary of Data

Experiment.	δ K Values. x 10^4 Habib	Nablo	δ %	K %
73 -β	δ_β (73) K_L = 435		6.4 $\pm$ 1.2	68
	δ_γ (388) K_L	1050		
	δ_γ (485) K_L = 292		4.3 $\pm$ 1.4	
139-β	δ_β (139) K_L = 75 $\pm$ 10		8.7 $\pm$ 0.8	8.6 $\pm$ 0.2
	δ_γ (322) K_L = 22 $\pm$ 3	101	2.6 $\pm$ 0.4	
	δ_γ (?) K_L = 10 $\pm$ 2		1.2 $\pm$ 0.2	
107 -β	(247) K_L = 15 $\pm$ 3	21 $\pm$ 5		
177 -β	(315) K_K = 18 $\pm$ 4	19 $\pm$ 5		
281 -β	(281) K_K = 25 $\pm$ 2	25 $\pm$ 2		
322 -β	(460) K_K = 20 $\pm$ 3	20 $\pm$ 2		7.6 $\pm$ 1.5
460 -β	(460) K_K = 23 $\pm$ 3	15 $\pm$ 1		

spectra were simple except perhaps for the 107L-β group. The suspicion that another beta group is in coincidence with this transition finds support in the discrepancy between the values of δ_K measured here and the intensity reported by Nablo. However no explanation has been found for the discrepancy between the two values of δ_K for the 460 kev transition. For the 322K-β, the value of δ was known from the 139L-β experiments so that α_K 322K could be determined.

(xi) Transition Intensities and Multipole Assignments.

Two lists of gamma ray intensities measured in this laboratory are available to the author. The first of these, reported in Nablo's Ph.D. thesis, presents the results of an investigation with a large Siegbahn double focussing spectrometer using external conversion. The intensity calibration curve used had been established by Nablo for work in Ir^{194} and was known to be reliable above $B\rho = 2500$. He extrapolated the curves into the low energy region in order to interpret the results on osmium. The intensities presented in the paper by Nablo Johns, Artna, and Goodman, are based on Nablo's results modified to fit Goodman's scintillation counter intensity measurements on the stronger gamma rays. In this paper there exists a serious discrepancy between the gamma and beta ray intensity scales. The present work seems to support Nablo's thesis results and casts serious doubts on the validity of the scintillation counter measurements. Nablo's original measurements gave relative intensities which he normalized to fit the beta intensities found from a Fermi analysis.

Since the results presented in the last section include absolute intensity measurements for the 322 and 388 kev transitions, it is now possible to

	Quantum Intensities Normalized x 10^4		Number of Conversion Electrons x 10^4			δ	α_K	α_K	α_L	α_L	Assignment
	Nablo	Habib.	K	L	M	%	M1	E2	M1	E2	
73			...	727		10.7 ± 1.2	...	...	1.92	13.5	E2
107			...	.15		0.25 to 1.2	4.7	0.69	0.68	2.4	
139			...	75	33	12.5 ± 1	2.2	0.42	0.32	0.72	M1
170	13					0.3					
177	17		18	5	...	0.4	1.00	0.22	0.16	0.22	M1
196	13					0.2					
243	17					0.25					
248	19		7	1	...	0.2	0.41	.097	0.063	0.051	M1 + E2
251	36					0.4					
278	40					0.5					
			25	6			0.29	0.073	0.045	0.033	M1 + E2
281	160					1.8					
288	48					0.5					
299	110		4	...	...	1.1	0.24	0.061	0.038	0.026	E2
314	53					0.6					
322	230	230	20	5	...	2.6	0.20	0.052	0.032	0.021	M1 + E2
362	158		3	1		1.6	0.14	0.038	0.022	0.013	E2
388	330	320	7	4		3.3	0.12	0.034	0.018	0.010	E2
460	1440		23	4		14.6	0.078	0.022	0.011	0.008	E2
485	100					1.0					
559	720					7.3					

TABLE 4

renormalize Nablo's data. This has been done in Table 4, column 2, using the 322 quantum intensity as a standard. Columns 4, 5, and 6 show conversion electron intensities. Wherever possible the values from present experiments have been used. The remainder came from the work of Nablo and Artna. The transition probabilities, column 7, follow directly from the gamma ray and conversion electron intensities for those cases where both of them are known. For the cases where the conversion electrons were not observed, estimates of their intensities have been made on the assumption that they are M1 + E2 mixtures. In the 107 kev transition only the $\delta \mathfrak{K}_L$ is known, so the values quoted for δ represents the limits possible for pure M1 and E2. The values of the conversion coefficients for M1 and E2 transitions for the K and L shells are listed in columns 8 - 11 and are taken from Rose's tables. Finally, multipole assignments for the stronger transitions are made.

(xii) The Decay Scheme

Figure 33 presents a decay scheme based on these measurements which accounts for all the gamma rays save the weak 251 and 288 kev transition. The intensities and energies of all the transitions are shown on the figure. The arrangement of levels is that given by Nablo et al except for the 613 kev level. There is now no doubt about the existence of all the levels shown except the 362 and the 661 kev levels, so these two levels are placed on the right hand side of the figure.

The presence of three weakly populated levels at 246, 281 and 317 kev levels have been strongly established by these experiments. The partial beta

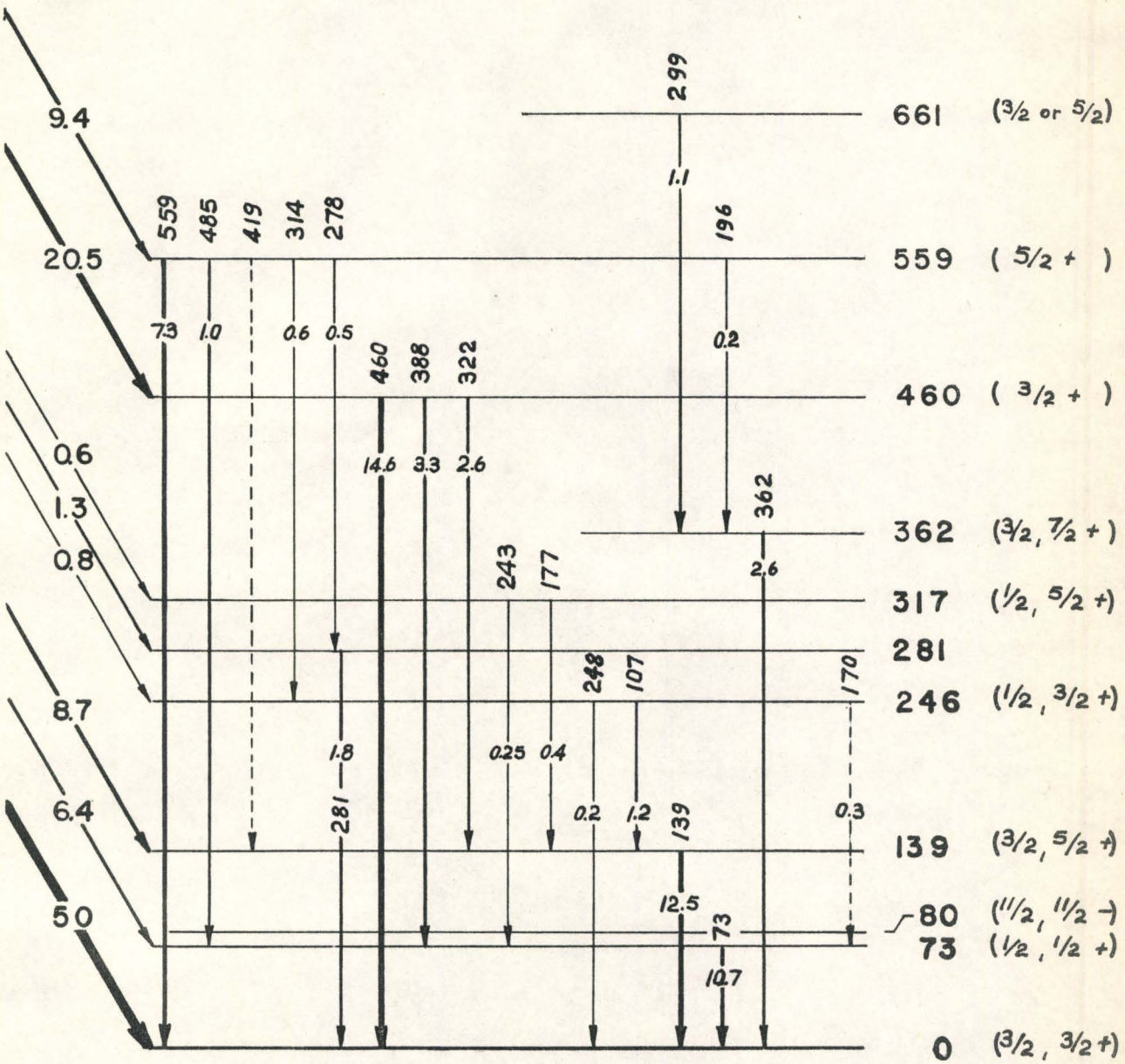
9.4
20.5
0.6
1.3
0.8
8.7
6.4
50
559
485
419
314
278
299
196
460
388
322
362
243
177
248
107
170
281
139
80
73
661 (3/2 or 5/2)
559 (5/2 +)
460 (3/2 +)
362 (3/2, 7/2 +)
317 (1/2, 5/2 +)
281
246 (1/2, 3/2 +)
139 (3/2, 5/2 +)
80 (11/2, 11/2 −)
73 (1/2, 1/2 +)
0 (3/2, 3/2 +)
7.3
1.0
0.6
0.5
1.1
0.2
14.6
3.3
2.6
2.6
1.8
0.25
0.4
0.2
1.2
0.3
12.5
10.7

FIG. 33

spectra feeding each of these levels have been observed. In the case of the 246 and 281 kev levels, these spectra are complex indicating feeding from a higher level in the 550 kev region. On the other hand the beta spectrum to the 317 kev level is simple at least down to 300 kev, thus indicating no feeding from levels below 800 kev. This fact makes it necessary to reject the Nablo assignment of the 299 kev transition as between the 613 and 317 kev levels. This takes away the main support for the existence of the 613 kev level. The suggestion of a level at 362 kev is based on the presence of the fairly strong 362 kev transition and the fact that a level near this value is known from Coulomb excitation work (40). Such a level must have spin 7/2 and can therefore not be fed directly by beta decay. In order to provide the necessary feeding, the 299 kev transition has been used and this introduces a new level at 661 kev. This argument is very tenuous and cannot be taken too seriously. It is unfortunate that the low intensities of the internal conversion lines of the 299 or 362 kev transition prevented a direct test of this assignment.

The intensities are based on coincidence measurements of the partial beta spectra, which gave absolute values for the beta groups to the 73 and 139 kev levels, and the absolute intensities of two other transitions. The beta intensities to the other levels have been calculated from the decay scheme and the transition probabilities discussed in section (xi) above. There is a large measure of disagreement between the beta intensities and those published by Nablo et al (39) but there is fair agreement with Nablo's thesis values. These values, based on a Fermi analysis of the complete spectrum indicates beta transitions as follows:

38% to the ground state; 26% to the 73, 9% to the 139, 9% to the 281, 11% to the 460 and 7% to the 538 kev levels. An analysis of a spectrum into so many groups is very subjective, and it is possible without doing violence to his data, to remove the intensity of the 281 group and add this to the 460 and 558 to give good agreement with the present work. In a similar way, the relative intensities to the three lower levels can be adjusted to agree with the present data.

An independent check on the correctness of these intensity measurements can be obtained from the measurement of the photon intensity of the 139 kev transition described by Nablo et al (39). They obtain a value of 3.1% for this gamma ray. From the present work, using the total intensity of the 139 kev transition as 10.7% and the multipole assignment as M1, a value of 3.3% is obtained for this gamma ray. The $\log_{10} ft$ values for the beta transitions to various levels are shown in the table below:

Level	Log ft.
0	7.4
73	8.2
139	8.1
246	9.0
281	8.7
314	9.0
362	>9.0
460	7.1
559	7.3

The transitions to the 460 and 559 kev levels seem to be favoured over the others by a factor of about 10. However all the beta transitions fall in the first forbidden region.

(xiii) Spins and Parities

From the Nilsson model (41) and the systematics of nuclei, it is clear

that the spin of Os^{193} is 3/2 with negative parity. This model also predicts the presence of low lying levels of spins, 3/2+, 1/2+, 11/2 - in Ir^{191}, Au^{197}. These levels have been found in all of these nuclei (42). It is clear that the ground state of Ir^{193} is a 3/2+ and that the 73 kev level is 1/2+. The 11/2- level has been found at 80 kev by these authors. Since nearly all these levels are populated by beta transitions, their spins must be 1/2, 3/2 or 5/2, with presumably positive parity. Negative parity states would lead to a number of E1 transitions, in contrast to the results of the internal conversion data. Unfortunately this makes it very difficult to assign unique spins to any but the lowest lying levels. One would not expect any transitions to the 80 kev level since those would be of a multipolarity M2 or higher.

The ground state spin of Ir^{193} has been measured to be 3/2 by Mach (43) and the shell model predicts positive parity. Coulomb excitation measurements (40) have identified rotational levels based on this state at 139 and 368 kev. Following this lead, spins of 5/2 and 7/2 have been assigned to the 139 and 362 kev levels. If one applies the appropriate rotational formula:

$E_{rot} = \frac{\hbar^2}{2j} I(I+1)$ to the first two levels one gets a value of $\frac{\hbar^2}{2j} = 27.5$ kev

Using this to calculate the position of the 7/2 level leads to a value of 330 kev in poor agreement with the expected value of 362 kev. However, unless the nucleus is highly deformed the expression for the energy above should be modified by a term proportional to $I^2 (I+1)^2$ (45), and is characteristic of the rotation-vibration interaction (45).

Another rotational sequence of levels may be the 73 (1/2+) 246 (3/2+)

314 (5/2+)levels. For these we must use the formula.

$$E_{rot} = \frac{\hbar^2}{2J}\left[I \quad (I+1) + a\ (-1)\ (I+1/2)\ (I+1/2)\right]$$ because it is based on a 1/2 state.

Here we find that $\frac{\hbar^2}{2j}$ = 36 kev, and a = 0.61.

The moment of inertia is therefore different for the ground state and this is to be expected for odd A nuclei. (44)

It is not possible to draw reasonable conclusions about the spins and parities of the other levels.

One might speculate as follows:

(i) The 460 kev and 559 kev levels are both vibrational states based on a ground state (K = 3/2 I = 3/2). An intrinsic vibration of spin 2 coupled to this particle motion would lead to possible levels described by (3/2, 7/2), (3/2 5/2), (3/2 3/2), (3/2 1/2) The 460 kev level must be (3/2, 5/2) or (3/2, 7/2) if the E2 character of the 388 kev line is to be believed. The 559 kev level could have any of the spin values 1/2, 3/2, 5/2. This description of the levels is attractive because both the 460 and 559 kev transitions have very similar decay patterns with the radiations of E2 character characteristic of vibrational spectra. It is also attractive because of the similarity of the ft values for beta decay to their states and the ground state. This assignment has been chosen for the decay scheme.

(ii) The 559 kev level may be the second member of rotational band based on the 460 level. In this case the 460 level must be described as (3/2, 3/2) and the 559 as (3/2, 5/2). The moment of inertia obtained for this picture is quite close to that for the ground state, but the decay pattern does not offer much support for this view. (iii) No speculation concerning the 281 or 661 kev levels seems to be profitable.

CONCLUSIONS

The experiments described in this thesis have demonstrated the usefulness of the electron-electron coincidence spectrometer in studying complex beta spectra. The performance of the instrument has come up well to expectations and is slightly better than that of the prototype constructed by T. R. Gerholm. Its usefulness can be greatly extended by replacing one lens by a gamma ray spectrometer, and feeding the output of the spectrometer to a multichannel pulse height analyser gated by pulses from the electron detector. This will reduce the time required for an experiment by several orders of magnitude.

In addition, its potentialities for the measurements of short lifetimes have not been exploited but it should be ideal for these determinations. The Os^{193} spectrum proved to be a very severe test of the instrument since the low specific activity of the irradiated osmium made it impossible to use strong sources, and because the low energy spectrum was so seriously masked by the Os^{191} spectrum. The results of the experiments led to essential confirmation of the decay scheme already published. However the position of the levels at 246, 281 and 317 are much more securely established than they had been before and the intensities of the beta and gamma group much more securely known.

As a consequence of these experiments, Goodman is preparing to repeat the scintillation counter measurement, to see if the discrepancy in intensities can be removed.

BIBLIOGRAPHY

(1) O. von Baeyer and O. Hahn. Phys. Zeit. 11, 488, 1910.
Phys. Zeit. 12, 273, 1911.
Phys. Zeit. 13, 264, 1912.

(2) J. Chadwick. Verh. d. D. Phys. Ges. 16, 383.

(3) E. Rutherford. Phil. Mag. 26, 717, 1913.
Phil. Mag. 28, 281, 1814.

(4) E. Rutherford, J. Chadwick, C. D. Ellis. Radiations from radioactive substances. Chapter XII. Cam. Univ. Press. 1951.

(5) C. L. Cowan, F. Reines et al. Science 124, 103-104, 1956.

(6) T. D. Lee and C. N. Yang. Phys. Rev. 104, 254, 1956.

(7) F. T. Porter, M. S. Freedman, T. B. Novey, F. Wagner. Phys. Rev. 98, 214L. 1955.

(8) M. E. Rose. Internal Conversion coefficients. North Holland Publ. Co., 1958.

(9) O. Haxel, J. H. D. Jensen and H. E. Suess. Phys. Rev. 75, 1766L. 1949.
Z. Physik 128, 295, 1950.

(10) M. G. Mayer. Phys. Rev. 78, 16, 1950.
Phys. Rev. 78, 22, 1950.

(11) A. Bohr and B. R. Mottelson. Kgl. Danske Videnskab. Selskab. Mat.-Fys. Medd. vol. 27, no. 16, 1953.

(12) A. S. Davydov and G. F. Philipov. Nuc. Physics 8, 237, 1958.

(13) Kai Siegbahn. Beta and Gamma Ray Spectroscopy. Chap. iii., Amsterdam, North Holland Publ. Co., 1959.

(14) E. Persico and C. Geoffrion. Rev. Sci. Instr. 21, 945, 1950.

(15) O. von Baeyer and O. Hahn. Phys. Zeit. 11, 488, 1910.

(16) J. Danyz. Le Radium 9, 1, 1912.
10, 4, 1913.

(17) N. Svartholm and K. Siegbahn. Ark. Mat. Fys. A33, no. 21, 1946; also Nature 157, 872, 1946.

(18) G. T. Ewan et al. Can. Journ. Phys. 37, 174, 1959.

(19) Lee Whiting and E. A. Taylor. Can. Journ. Phys. 35, 1, 1957.

(20) R. Tricker. Proc. Cam. Phil. Soc. 22, 454, 1924.

(21) J. DuMond, L. Bogart, J. Kohl, D. Muller, J. Witts. Calif. Inst. of Tech. Rep. no. 16, 1952.

(22) F. Schmidt. Rev. Sci. Instr. 23, 361, 1952.

(23) H. Slatis and K. Siegbahn. Ark. f. Fysik 1, no. 17, 339, 1949.

(24) H. de Waard. Thesis. Groningen University, 1954. Also, see ref. (13).

(25) T. R. Gerholm. Rev. Sci. Instr., vol. 26, no. 11, 1069-1072, 1955.

(26) K. Siegbahn. Beta and Gamma Ray Spectroscopy, appendix viii.

(27) S. Frankel. Phys. Rev. 73, 804, 1948.

(28) R. Nichols and E. Jensen. Phys. Rev. 94, 369, 1954.

(29) J. W. DuMond. Rev. Sci. Instr. 20, 160, 1949.

(30) E. Persico. Rev. Sci. Instr. 20, 191, 1949.

(31) P. Hubert. Physica XVIII, no. 12, 1952.

(32) T. R. Gerholm. Ark. f. Fysik, 11, no. 2, 55, 1956.

(33) J. Lindgren. Nuclear Instruments. 3, 104, 1958.

(34) Y. Ramberg and A. E. Blaugrund. Rev. Sci. Instr. 28, 286, 1957.

(35) R. E. Bell, R. L. Graham and H. E. Petch, Can. Journ. Phys., 30, 35, 1952.

(36) M. Bunker, R. Canada, A. C. G. Mitchell. Phys. Rev. 79, 610, 1950.

(37) J. M. Cork, J. M. LeBlanc, W. H. Nester, D. W. Martin, M. K. Brice. Phys. Rev. 90, 444, 1953.

(38) H. de Waard. Physica 20, 41, 1954.

(39) S. V. Nablo, M. W. Johns, A. Artna and R. H. Goodman. Can. Journ. of Phys. 36, 1409, 1958.

(40) R. H. Davis, A. S. Divatia, D. A. Lind, R. D. Moffat. Phys. Rev. 103, 1801, 1956.

(41) S. G. Nilsson. Kgl. Danske Videnskab. Selskab. Mat.-Fys. Med. vol. 29, no. 16, 1955.

(42) F. Boehm and P. Marmier. Phys. Rev. 105, 974, 1957.

(43) J. E. Mach. Revs. Mod. Phys. 22, 64, 1950.

(44) B. R. Mottelson, S. G. Nilsson. Kgl. Danske Videnskab. Selskab. Mat.-Fys. Skrifter, vol. 1, no. 8, 1959.

(45) G. Alaga, K. Alder, A. Bohr and B. R. Mottelson. Klg. Danske Videnskab. Selskab. Mat.-Fys. Med. vol. 29, no. 9.

(46) V. F. Weisskopf. Phys. Rev. 83, 1073, 1951.